Classifications of ideal 3D elastica shapes at equilibrium

Olivier Ameline, Sinan Haliyo, Xingxi Huang, and Jean A. H. Cognet

Citation: Journal of Mathematical Physics **58**, 062902 (2017); doi: 10.1063/1.4989556
View online: http://dx.doi.org/10.1063/1.4989556
View Table of Contents: http://aip.scitation.org/toc/jmp/58/6
Published by the American Institute of Physics

JOURNAL OF MATHEMATICAL PHYSICS **58**, 062902 (2017)

Classifications of ideal 3D elastica shapes at equilibrium

Olivier Ameline,[1,2] Sinan Haliyo,[1] Xingxi Huang,[1,2] and Jean A. H. Cognet[2,a)]
[1]*Sorbonne Universités, UPMC University Paris 06, UMR 7222, ISIR, BC 173, 4 Place Jussieu, F-75252 Paris Cedex 05, France*
[2]*Sorbonne Universités, UPMC University Paris 06, UMR 8237, LJP, BC 114, 4 Place Jussieu, F-75252 Paris Cedex 05, France*

(Received 30 September 2016; accepted 9 June 2017; published online 30 June 2017)

We investigate the equilibrium configurations of the ideal 3D elastica, i.e., inextensible, unshearable, isotropic, uniform, and naturally straight and prismatic rods, with linear elastic constitutive relations. Infinite solution trajectories are expressed analytically and classified in terms of only three parameters related to physical quantities. Orientation of sections and mechanical loading are also well described analytically with these parameters. Detailed analysis of solution trajectories yields two main results. First, all particular trajectories are completely characterized and located in the space of these parameters. Second, a general geometric structure is exhibited for every ideal 3D elastic rod, where the trajectory winds around a core helix in a tube-shaped envelope. This remarkable structure leads to a classification of the general case according to three properties called chirality components. In addition, the geometry of the envelope provides another characterization of the ideal 3D elastica. For both results, the domains and the frontiers of every class are plotted in the space of the parameters. *Published by AIP Publishing.* [http://dx.doi.org/10.1063/1.4989556]

I. INTRODUCTION

Elastic rod models are relevant in many diverse problems at different scales, among which the deformation of guidewires in interventional radiology,[1] the anguilliform swimming simulation,[2] and the study of cell mobility through flagella.[3] Recently, carbon nanotubes provoked a great interest in micro- and nano-scale engineering, and continuum mechanics beam models proved to be useful to simulate their behavior.[4] Even the important development of micro-electro-mechanical systems (MEMS) can lead to numerous problems treated with elastic rods, as the wrong actuation of micro-cantilevers due to capillarity.[5] In biochemistry, the elastic deformations of rods provide a good model for filamentary structures such as DNA molecules,[6–10] bacterial fibers,[11,12] and proteins.[13]

Although it has been studied for over two centuries, the static equilibrium of elastic rods in large deformation remains not entirely solved. There were various works that successfully obtained the 3D shape equations in terms of a set of parameters,[14–16] but these parameters are not always easily related to physical quantities. It is also difficult to obtain an intuitive parametrization, with clear effects on the geometry of the rod. To improve the knowledge of elastic rod configurations, it is necessary to take interest in the corresponding bifurcation problem.[17] In this perspective, authors proposed classifications of particular cases as planar elastica,[18] buckling,[19] closed shapes,[20–22] helices,[23] and clamped elastica.[24,25] A step toward a general geometric classification was accomplished by regrouping the majority of cases in one formalism.[26] Still the parameters used, roots of a third degree polynomial, have no immediate physical meaning. Moreover, a graphic representation of the frontiers between the classes of solutions would improve the understanding of the bifurcation possibilities. Even though such kind of cartography could be proposed, it is still lacking. Then, apart from particular cases, elastic rod geometries were not completely characterized.

a)Electronic mail: jean.cognet@upmc.fr

Yet, a geometric structure has emerged, where the trajectory winds around an average helix.[26,27]

In this paper, we use the formalism of Landau *et al.*[28] to classify all analytical solutions of ideal 3D elastica. This formalism yields three parameters $\{\lambda, t_P, a\}$ that are related to physical quantities. These three parameters are sufficient to define analytically all infinite rod trajectories. Only the case where no force is acting on the rod is treated separately in the supplementary material, using two parameters that are very similar to λ and t_P. In all cases, each set of parameters refers to a unique solution, except in a line interval in space $\{\lambda, t_P, a\}$ where two solutions are possible. In addition to the trajectory, these parameters are relevant to describe analytically the orientation of sections and mechanical loading. Furthermore, the global reference frame chosen by Landau makes the solutions conveniently and automatically written in a cylindrical coordinate system with axis z. Thus, it is very convenient to focus on the geometry of the rod and not on its position and orientation in space.

With this setting, two main results are obtained. First, we locate each particular trajectory in the space described by parameters $\{\lambda, t_P, a\}$: straight rods, circular trajectories, planar elastica, helices, homoclinic shapes, and closed shapes. Second, we exhibit a geometric structure of every 3D elastic rod at equilibrium: they all wind around a core helix of axis z and are contained within a tube-shaped envelope with circular section. This structure leads to a general classification of ideal 3D elastica according to three chiral properties introduced in this article. We have plotted the surfaces that delimit the corresponding chiral classes in the $\{\lambda, t_P, a\}$ space. It also yields analytical expressions of infinite trajectories in terms of three other parameters $\{\rho_H, \rho_G, a\}$ that are clearly related to the geometry of the tube-shaped envelope. Thus, another general characterization of ideal 3D elastica is obtained, according to the pitch and radii of this envelope. These results provide a precise analytic and geometric representation of the global bifurcation problem in the general case of ideal elastica.

In Sec. II, we expose the formalism to express the solutions of ideal 3D elastica, taking into account all singular cases for numeric implementation. In Sec. III, we obtain the domain of definition of the parameters, i.e., the region of space $\{\lambda, t_P, a\}$ for which there exist solution rod shapes. Then, in Sec. IV, particular rod geometries are located precisely in this region. Finally in Sec. V, we present the classification of the general case according to chiral properties and the characterization according to the geometry of the tube-shaped envelope.

All computations and graphics were executed with Wolfram Mathematica 10.[29] Figures 3, 5, 7, and 9 can be viewed interactively in the supplementary material. This requires Wolfram CDF Player, freely downloadable at http://www.wolfram.com/cdf-player/.

II. PRESENTATION OF THE FORMALISM

A. System of mechanical equilibrium

Ideal elastica[24] refers to inextensible, unshearable, isotropic, uniform, and naturally straight and prismatic rods made of a hyper-elastic material with linear constitutive relations. Such rods can be described by the Cosserat theory.[17] We consider them as parts of generic geometries characterized by the infinite trajectory $\{\boldsymbol{r}(s) = \boldsymbol{OG}(s), s \in \mathbb{R}\}$ of their centre line, together with a local reference frame $\{G(s), \boldsymbol{d}_1, \boldsymbol{d}_2, \boldsymbol{d}_3\}$ called the Darboux frame and giving the orientation of sections. This description is made in a global reference frame $\{O, \boldsymbol{e}_i, \boldsymbol{e}_j, \boldsymbol{e}_k\}$. Noting with a prime $'$ the derivative with respect to s, inextensibility and unshearability write $||\boldsymbol{r}'(s)|| = 1$ and imply that the curvilinear abscissa is also the arc length. Furthermore, ideal elastica hypotheses lead to sections perpendicular to the trajectory; thus the Darboux frame is obtained by a rotation of the Frenet reference frame $\{G(s), \boldsymbol{n}, \boldsymbol{b}, \boldsymbol{t}\}$ around the tangent $\boldsymbol{t}$,

$$\boldsymbol{r}'(s) = \boldsymbol{t}(s) = \boldsymbol{d}_3(s) \quad \forall\, s \in \mathbb{R}. \tag{2.1}$$

Figure 1 defines the Euler angles $\{\psi, \theta, \varphi\}$ which transform bases $\{\boldsymbol{e}_i, \boldsymbol{e}_j, \boldsymbol{e}_k\}$ to local Darboux bases $\{\boldsymbol{d}_1, \boldsymbol{d}_2, \boldsymbol{d}_3\}$, so that

$$\boldsymbol{d}_\mu = E_{\mu,1}\boldsymbol{e}_i + E_{\mu,2}\boldsymbol{e}_j + E_{\mu,3}\boldsymbol{e}_k \quad \forall\, \mu \in \{1, 2, 3\} \tag{2.2}$$

with

$$\boldsymbol{E}=\begin{pmatrix} \cos\psi\cos\theta\cos\varphi-\sin\psi\sin\varphi & \sin\psi\cos\theta\cos\varphi+\cos\psi\sin\varphi & -\sin\theta\cos\varphi \\ -\cos\psi\cos\theta\sin\varphi-\sin\psi\cos\varphi & -\sin\psi\cos\theta\sin\varphi+\cos\psi\cos\varphi & \sin\theta\sin\varphi \\ \cos\psi\sin\theta & \sin\psi\sin\theta & \cos\theta \end{pmatrix}. \tag{2.3}$$

In (2.2), $E_{\mu,\nu}$ denotes the coefficient of matrix $\boldsymbol{E}$ at line μ and column ν.

The angular deformation $\boldsymbol{\Omega}(s)$ of the rod is defined as the angle density vector

$$\boldsymbol{\Omega}(s)=\psi'(s)\,\boldsymbol{e}_k+\theta'(s)\,\boldsymbol{v}_2(s)+\varphi'(s)\,\boldsymbol{d}_3(s), \tag{2.4}$$

where $\boldsymbol{v}_2(s)=-\sin(\psi)\,\boldsymbol{e}_i+\cos(\psi)\,\boldsymbol{e}_j$. $\boldsymbol{\Omega}(s)$ is also called the Darboux vector and can be defined equivalently by

$$\boldsymbol{d}'_\mu(s)=\boldsymbol{\Omega}(s)\times\boldsymbol{d}_\mu(s)\quad\forall\,\mu\in\{1,2,3\}. \tag{2.5}$$

This vector can be written in the Frenet frame as follows:[28]

$$\boldsymbol{\Omega}(s)=\kappa(s)\boldsymbol{b}(s)+\Omega_t\boldsymbol{t}(s), \tag{2.6}$$

where Ω_t is the constant physical twist density and $\kappa(s)$ is the local curvature, defined in the inextensible case as

$$\kappa(s)=||\boldsymbol{t}'(s)||=||\boldsymbol{r}''(s)||. \tag{2.7}$$

Calling $\boldsymbol{F}$ the force and $\boldsymbol{M}$ the moment that act across each section, the mechanical equilibrium is given by[28]

$$\begin{cases}\boldsymbol{F}'(s)=\boldsymbol{0}, & \text{(2.8a)}\\ \boldsymbol{M}'(s)+\boldsymbol{t}(s)\times\boldsymbol{F}(s)=\boldsymbol{0}. & \text{(2.8b)}\end{cases}$$

Considering only rods with isotropic cross sections, $K_0=K_1=K_2$ denotes the bending rigidity and K_3 the twisting rigidity. The integration of system (2.8) from 0 to s, together with the hyper-elastic constitutive relations, lead to

$$\begin{cases}\boldsymbol{F}(s)=\boldsymbol{F}=\boldsymbol{cst}, & \text{(2.9a)}\\ \boldsymbol{M}(s)=K_0\kappa(s)\boldsymbol{b}(s)+K_3\Omega_t\boldsymbol{t}(s)=\boldsymbol{F}\times\boldsymbol{r}(s)+\boldsymbol{M_O}, & \text{(2.9b)}\end{cases}$$

with

$$\boldsymbol{M_O}=-\boldsymbol{F}\times\boldsymbol{r}(0)+\boldsymbol{M}(0). \tag{2.10}$$

(2.9) can also be written as an s-independent Hamiltonian system,[21] whose constant Hamiltonian is the total energy density

$$H=\frac{1}{2}\boldsymbol{M}\cdot\boldsymbol{\Omega}+\boldsymbol{F}\cdot\boldsymbol{d}_3. \tag{2.11}$$

B. Constants of the problem

Four constants $\boldsymbol{F}$, $\boldsymbol{M_O}$, $\boldsymbol{M}(s)\cdot\boldsymbol{t}$, and H can be identified in (2.9). When $\boldsymbol{F}\neq\boldsymbol{0}$, Landau's formalism reduces these constants to four scalar quantities, through a judicious choice of the initial curvilinear abscissa and of the reference frame. Then, it introduces three combinations $\{\lambda, t_P, a\}$ of these constants that prove sufficient to express the solutions analytically.[16,28] Case $\boldsymbol{F}=\boldsymbol{0}$ is treated in the supplementary material.

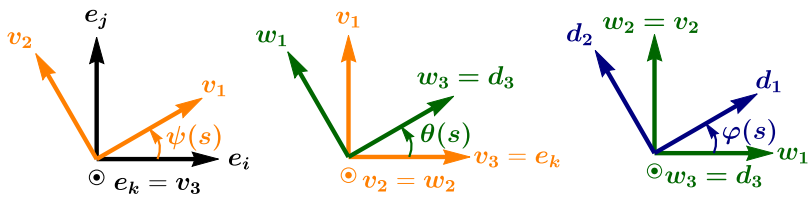

FIG. 1. Euler angles: $(\psi,\varphi)\in[\,0,2\pi\,[^2$ and $\theta\in[0,\pi]$.

1. Origin of curvilinear abscissa

It has been demonstrated in many works that for all ideal elastic rods, the quantity $\boldsymbol{F}\cdot\boldsymbol{d}_3$ has a minimal value.[16,19,26] With (2.6), (2.9b), and (2.11), it implies the existence of an abscissa for which $||\boldsymbol{M}||$ is maximal: this abscissa is chosen as the reference $s=0$. From (2.8b), vectors $\boldsymbol{F}$, $\boldsymbol{d}_3(0)$, and $\boldsymbol{M}(0)$ are coplanar with this choice. Thus, as $\boldsymbol{n}(0)$ is orthogonal to $\boldsymbol{d}_3(0)$ and $\boldsymbol{M}(0)$, it is also orthogonal to $\boldsymbol{F}$. This interesting property is used to propose a judicious reference frame, in which elastic trajectories are conveniently written.

2. Global reference frame

Noting $F>0$ the norm of the constant vector force $\boldsymbol{F}$, the global reference frame $\{O,\boldsymbol{e}_i,\boldsymbol{e}_j,\boldsymbol{e}_k\}$ is chosen by imposing

$$\boldsymbol{e}_k=\frac{1}{F}\boldsymbol{F},\quad \boldsymbol{e}_i=-\boldsymbol{n}(0),\quad \boldsymbol{r}(0)=\frac{1}{F}\left(\boldsymbol{M}(0)\cdot\boldsymbol{e}_j\right)\boldsymbol{e}_i. \tag{2.12}$$

Note that the curvature κ is maximal at $s=0$, hence $\kappa(0)=0$ only occurs for straight rods. In this case, $\boldsymbol{n}(0)$ is not defined but the unit vector $\boldsymbol{e}_i$ can be chosen arbitrarily.

With this reference frame

$$\boldsymbol{M}(0)\cdot\boldsymbol{e}_i=K_0\kappa(0)\boldsymbol{b}(0)\cdot\boldsymbol{e}_i+K_3\Omega_t\boldsymbol{t}(0)\cdot\boldsymbol{e}_i=0 \tag{2.13}$$

and using Eqs. (2.9)–(2.13),

$$\boldsymbol{M_O}=(\boldsymbol{M}(0)\cdot\boldsymbol{e}_k)\,\boldsymbol{e}_k=(\boldsymbol{M}(s)\cdot\boldsymbol{e}_k)\,\boldsymbol{e}_k\quad\forall\, s\in\mathbb{R}. \tag{2.14}$$

As a result, this choice reduces the constant force $\boldsymbol{F}=F\boldsymbol{e}_k$ to a scalar quantity and cancels all components of $\boldsymbol{M_O}$ perpendicular to $\boldsymbol{F}$.

3. Landau's parameters $\{\lambda, t_P, a\}$

The first parameter λ is the component along $\boldsymbol{e}_k$ of the moment, divided by the force F,

$$\lambda=\frac{1}{F}\boldsymbol{M_O}\cdot\boldsymbol{e}_k=\frac{1}{F}\boldsymbol{M}(s)\cdot\boldsymbol{e}_k\quad\forall\, s\in\mathbb{R}. \tag{2.15}$$

The second parameter is the scaled physical twist density

$$t_P=\frac{1}{K_0}\boldsymbol{M}(s)\cdot\boldsymbol{t}=\frac{K_3}{K_0}\Omega_t\quad\forall\, s\in\mathbb{R}. \tag{2.16}$$

Finally, noting $\boldsymbol{M}^{\perp\boldsymbol{e}_k}=\boldsymbol{M}-(\boldsymbol{M}\cdot\boldsymbol{e}_k)\,\boldsymbol{e}_k$, the third parameter a is defined as

$$a=\frac{2}{F}\boldsymbol{F}\cdot\boldsymbol{t}+\frac{1}{K_0F}||\boldsymbol{M}^{\perp\boldsymbol{e}_k}||^2. \tag{2.17}$$

This dimensionless parameter can be seen as the sum of the contribution of traction (or compression) and of the component of the moment orthogonal to $\boldsymbol{e}_k$. With $\boldsymbol{r}^{\perp\boldsymbol{e}_k}=\boldsymbol{r}-(\boldsymbol{r}\cdot\boldsymbol{e}_k)\,\boldsymbol{e}_k$, Eqs. (2.9b), (2.12), and (2.14) lead to

$$||\boldsymbol{M}^{\perp\boldsymbol{e}_k}||=||\boldsymbol{F}\times\boldsymbol{r}||=||\boldsymbol{r}^{\perp\boldsymbol{e}_k}||F. \tag{2.18}$$

Using Eqs. (2.6), (2.9b), and (2.11), a can be written as

$$a=2\frac{H}{F}+\left(1-\frac{K_0}{K_3}\right)\frac{K_0}{F}t_P^2-\frac{F}{K_0}\lambda^2, \tag{2.19}$$

so that it is a combination of the four constants F, $\boldsymbol{M_O}\cdot\boldsymbol{e}_k$, $\boldsymbol{M}(s)\cdot\boldsymbol{t}$, and H.

C. Elastic trajectories

Equation (2.9b) can be written as follows:

$$\boldsymbol{M}(s)=K_0\,\boldsymbol{r}'(s)\times\boldsymbol{r}''(s)+K_0\,t_P\,\boldsymbol{r}'(s)=\boldsymbol{F}\times\boldsymbol{r}(s)+\lambda\boldsymbol{F}. \tag{2.20}$$

Solutions of (2.20) give all possible elastic trajectories $\boldsymbol{r}(s)$. They can be expressed analytically in terms of the three parameters $\{\lambda, t_P, a\}$. With this objective, the units of force and length

are changed to write (2.9) more generally for every F, K_0, and K_3. Then, the cylindrical coordinates (ρ, ϕ, z) are identified as the most convenient ones to describe the solutions. The integration of the resulting system requires firstly to solve a third-degree polynomial equation: we give the expressions of the corresponding roots. Finally, the analytical solutions of the trajectory of the centre line are expressed. We take special interest in every particular cases that may be usually ignored.

1. Dimensionless equation

In Ref. 16, $\sqrt{2K_0/F}$ is judiciously proposed as the unit of length. We prefer to choose $\widetilde{\mu} = \sqrt{K_0/F}$ because it leads to the most convenient set of parameters $\{\lambda, t_P, a\}$ to classify the solutions. We also take F as the unit of force. From here, each quantity with a dimension is denoted with a tilde $\widetilde{\ }$, in order to distinguish it from its dimensionless form. The derivative with respect to the dimensionless abscissa s is indicated by a dot, instead of a prime $'$ for the derivative with respect to the dimensionalized abscissa $\widetilde{s}$,

$$\begin{gathered}\widetilde{\boldsymbol{F}} = \widetilde{F}\,\boldsymbol{F}, \quad \widetilde{\boldsymbol{M}} = \widetilde{\mu}\widetilde{F}\,\boldsymbol{M}, \quad \widetilde{\boldsymbol{r}} = \widetilde{\mu}\,\boldsymbol{r}, \\ \widetilde{\kappa} = (1/\widetilde{\mu})\kappa, \quad \widetilde{\lambda} = \widetilde{\mu}\lambda, \quad \widetilde{t_P} = (1/\widetilde{\mu})t_P, \quad X' = (1/\widetilde{\mu})\dot{X}.\end{gathered} \tag{2.21}$$

Under this nondimensionalization, Eq. (2.20) becomes

$$\boldsymbol{M}(s) = \boldsymbol{\Omega}^{\perp t} + t_P\,\boldsymbol{t} = \dot{\boldsymbol{r}} \times \ddot{\boldsymbol{r}} + t_P\,\dot{\boldsymbol{r}} = \boldsymbol{e}_k \times \boldsymbol{r} + \lambda\,\boldsymbol{e}_k. \tag{2.22}$$

2. Cylindrical coordinates

The dimensionless Cartesian coordinates are noted (x, y, z), such as

$$\boldsymbol{r}(s) = x(s)\boldsymbol{e}_i + y(s)\boldsymbol{e}_j + z(s)\boldsymbol{e}_k. \tag{2.23}$$

Solutions of (2.22) are conveniently expressed with the cylindrical coordinates (ρ, ϕ, z),

$$x = \rho\cos(\phi), \quad y = \rho\sin(\phi). \tag{2.24}$$

Noting $u = \rho^2$, Eq. (2.22) yields[16]

$$\begin{cases} \dot{z}(s) = \dfrac{1}{2}(a-u), & \text{(2.25a)} \\ \dot{\phi}(s) = \left(t_P - (a-u)\dfrac{\lambda}{2}\right)\dfrac{1}{u}, & \text{(2.25b)} \\ \dot{u}(s) = \pm\sqrt{p_3(u)}. & \text{(2.25c)} \end{cases}$$

$p_3(u)$ is a polynomial of the third degree, with roots $\{u_1, u_2, u_3\}$, defined as

$$p_3(u) = -\left(\varepsilon_3 u^3 + \varepsilon_2 u^2 + \varepsilon_1 u + \varepsilon_0\right) = -(u-u_1)(u-u_2)(u-u_3), \tag{2.26}$$

where

$$\varepsilon_0 = (\lambda a - 2t_P)^2, \quad \varepsilon_1 = 4\lambda t_P - 2\lambda^2 a + a^2 - 4, \quad \varepsilon_2 = \lambda^2 - 2a, \quad \varepsilon_3 = 1. \tag{2.27}$$

3. Roots of $p_3(u)$

To integrate (2.25c), it is convenient to factorize $p_3(u)$, which requires to express its roots. These roots $\{u_1, u_2, u_3\}$ are related to the coefficients ε_k through

$$\begin{cases} u_1 + u_2 + u_3 = -\varepsilon_2 = 2a - \lambda^2, & \text{(2.28a)} \\ u_1u_2 + u_1u_3 + u_2u_3 = \varepsilon_1 = 4\lambda t_P - 2\lambda^2 a + a^2 - 4, & \text{(2.28b)} \\ u_1u_2u_3 = -\varepsilon_0 = -(\lambda a - 2t_P)^2 \le 0. & \text{(2.28c)} \end{cases}$$

The discriminant Δ of $p_3(u)$ is defined by

$$\Delta = \Delta(\lambda, t_P, a) = -(4p^3 + 27q^2), \tag{2.29}$$

where

$$p = p(\lambda, t_P, a) = -\frac{1}{3}\varepsilon_2^2 + \varepsilon_1, \quad q = q(\lambda, t_P, a) = \frac{2}{27}\varepsilon_2^3 - \frac{1}{3}\varepsilon_1\varepsilon_2 + \varepsilon_0. \tag{2.30}$$

The roots u_k ($k \in \{1, 2, 3\}$) are all real if and only if $\Delta \geq 0$, and in this case they are expressed as[30]

$$u_k = u_k(\lambda, t_P, a) = \frac{1}{3}(2a - \lambda^2) + 2\sqrt{-\frac{p}{3}}\cos\left(\frac{1}{3}\arccos\left(-\frac{q}{2}\sqrt{-\frac{27}{p^3}}\right) + \frac{2k\pi}{3}\right). \tag{2.31}$$

With this definition, we obtain real-ordered roots such that $u_1 \leq u_2 \leq u_3$. The case $p = 0$ may occur only when $\Delta = 0$ and leads to one triple root $u_k = (2a - \lambda^2)/3$.

4. Solutions

(2.25) has solutions if $\{u_1, u_2, u_3\}$ are real and under other conditions that are exposed in Sec. III. When $u_3 \neq 0$, these solutions are expressed in terms of elliptic functions and elliptic integrals of modulus m and characteristic n defined as

$$m = \frac{u_3 - u_2}{u_3 - u_1}, \quad n = \frac{u_3 - u_2}{u_3}. \tag{2.32}$$

The demonstration that $u_3 = 0$ corresponds to straight rods is in the pdf the supplementary material, Subsection SI A.

To obtain the solutions, the inverse of Eq. (2.25c) is integrated from u to u_3. This integration is achieved through a change of variable $\sin^2\Psi = (u_3 - u)/(u_3 - u_2)$ that we translate into

$$\Psi(s) = \mathrm{am}(c_\Psi s, m), \quad \text{with} \quad c_\Psi = \frac{1}{2}\sqrt{u_3 - u_1}, \tag{2.33}$$

where $\mathrm{am}(\cdot, m)$ denotes the Jacobi amplitude function. This results in[16]

$$\begin{cases} u(s) = u_3 - (u_3 - u_2)\mathrm{sn}^2(c_\Psi s, m), & \text{(2.34a)} \\ \phi(s) = \frac{1}{2}\lambda s + \frac{2t_P - \lambda a}{2c_\Psi u_3}\Pi(n, \Psi(s), m) + \phi_{cor}(s), & \text{(2.34b)} \\ z(s) = \frac{1}{2}(a - u_1)s - 2c_\Psi E(\Psi(s), m), & \text{(2.34c)} \end{cases}$$

where $\phi_{cor}(s)$ is defined as follows to take into account singularities when the trajectory intersects axis z,

$$\phi_{cor}(s) = \begin{cases} \left(\lfloor s/s_{per} - 1/2 \rfloor + 1\right)\pi & \text{if} \quad n = 1 \quad \text{and} \quad m \neq 1 \\ 0 & \text{otherwise} \end{cases}. \tag{2.35}$$

$\mathrm{sn}(\cdot, m)$ is the sinus function of Jacobi and $E(\cdot, m)$, $\Pi(n, \cdot, m)$ are the elliptic integrals of, respectively, the second and the third kind. See Appendix A for the expressions of the elliptic functions used in this article. $\lfloor \cdot \rfloor$ represents the floor function.

Note that when $m \neq 1$, the function $u(s)$ of (2.34a) is periodic with period

$$s_{per} = \frac{2K(m)}{c_\Psi}, \tag{2.36}$$

where $K(m) = F(\pi/2, m)$ is the complete elliptic integral of the first kind. Then, u_2 and u_3 are, respectively, the minimum and the maximum values of $u(s)$ and

$$u(0) = u_3, \quad u\left(s_{per}/2\right) = u_2. \tag{2.37}$$

The angular coordinate $\phi(s)$ of (2.34b) varies in $\mathbb{R}$, so that it is continuous when the trajectory does not intersect axis z. As $\phi(0) = 0$, the integer value of $\phi(s)/2\pi$ is the signed number of turns done by $\boldsymbol{r}^{\perp \boldsymbol{e}_k}$ around $\boldsymbol{e}_k$ from 0 to s (positive if the turns are achieved in the trigonometric orientation). When $n = 1$, which is equivalent to $u_2 = 0$, the term involving n in (2.34b) has to be removed. In this case, the corrective value $\phi_{cor}(s)$ is necessary to add π to $\phi(s)$ each time the trajectory intersects axis z.

System (2.34) gives the equations of almost all infinite elastic trajectories, parametrized by only three constants $\{\lambda, t_P, a\}$. For a complete overview of ideal elastica, we only need to add the straight rods obtained in Subsection IV A and the force-less configurations studied in the supplementary material.

D. Orientation of sections

There are two methods to define the physical orientation of sections. The first one is to express the Euler angles $\{\psi, \theta, \varphi\}$ that orientate $\{\boldsymbol{d}_1, \boldsymbol{d}_2, \boldsymbol{d}_3\}$ in $\{\boldsymbol{e}_i, \boldsymbol{e}_j, \boldsymbol{e}_k\}$. The second one is to express the angle ζ between the Darboux frame and the Frenet frame. Whatever the method is, the three parameters $\{\lambda, t_P, a\}$ are pertinent to define the orientation of sections: only two additional parameters $\{\varphi(0), K_3/K_0\}$ or $\{\zeta(0), K_3/K_0\}$ are needed.

1. Expressions of Euler angles

To express Euler angles, we first write the angular deformation $\boldsymbol{\Omega}$ in the Darboux frame,[31]

$$\Omega_1(s) = \boldsymbol{\Omega} \cdot \boldsymbol{d}_1 = \dot{\theta}\sin(\varphi) - \dot{\psi}\sin(\theta)\cos(\varphi), \tag{2.38a}$$

$$\Omega_2(s) = \boldsymbol{\Omega} \cdot \boldsymbol{d}_2 = \dot{\theta}\cos(\varphi) + \dot{\psi}\sin(\theta)\sin(\varphi), \tag{2.38b}$$

$$\Omega_3(s) = \boldsymbol{\Omega} \cdot \boldsymbol{d}_3 = \Omega_t = \dot{\psi}\cos(\theta) + \dot{\varphi}. \tag{2.38c}$$

We note $z_\theta = \cos(\theta) = \boldsymbol{t} \cdot \boldsymbol{e}_k = \dot{z}$. Non-dimensionalizing the definitions of $\widetilde{\lambda}$ and $\widetilde{t_P}$ in Sec. II B and using Eqs. (2.2), (2.22), and (2.38) yield

$$\begin{cases} \lambda = \left(1 + \left(\dfrac{K_3}{K_0} - 1\right) z_\theta^2\right) \dot{\psi} + \dfrac{K_3}{K_0} \dot{\varphi} z_\theta, & (2.39a) \\ t_P = \left(\dot{\psi} z_\theta + \dot{\varphi}\right) \dfrac{K_3}{K_0}. & (2.39b) \end{cases}$$

Then with Eq. (2.25a), we arrive at

$$\begin{cases} \dot{\psi}(s) = \dfrac{\lambda - t_P z_\theta}{1 - z_\theta^2}, & (2.40a) \\ \dot{\varphi}(s) = \left(\dfrac{K_0}{K_3} - 1\right) t_P + \dfrac{t_P - \lambda z_\theta}{1 - z_\theta^2}, & (2.40b) \\ z_\theta(s) = \dot{z}(s) = \dfrac{1}{2}(a - u). & (2.40c) \end{cases}$$

The solutions of this system are expressed in terms of elliptic functions[26] (see Appendix B),

$$\begin{cases} \psi(s) \equiv \psi(0) + \psi^+(s) + \psi^-(s) + \psi_{cor}(s) \quad [2\pi], & (2.41a) \\ \theta(s) = \arccos\left(\dfrac{a - u_3}{2} + \dfrac{u_3 - u_2}{2} \mathrm{sn}^2\left(c_\Psi s, m\right)\right), & (2.41b) \\ \varphi(s) \equiv \varphi(0) + (K_0/K_3 - 1) t_P\, s + \psi^+(s) - \psi^-(s) + \psi_{cor}(s) \quad [2\pi], & (2.41c) \end{cases}$$

with

$$\psi^+(s) = \frac{\lambda + t_P}{2 + a - u_3} \frac{1}{c_\Psi} \Pi\left(n^+, \Psi(s), m\right), \quad \psi^-(s) = \frac{\lambda - t_P}{2 - a + u_3} \frac{1}{c_\Psi} \Pi\left(n^-, \Psi(s), m\right). \tag{2.42a}$$

The characteristics n^+ and n^- are related to $\{u_1, u_2, u_3\}$ by

$$n^+ = \frac{u_3 - u_2}{u_3 - (a + 2)}, \quad n^- = \frac{u_3 - u_2}{u_3 - (a - 2)}. \tag{2.43}$$

When n^+ (respectively, n^-) has a vanishing denominator, Eq. (2.41) can be modified by suppressing the terms $\psi^+(s)$ (respectively, $\psi^-(s)$). The correction $\psi_{cor}(s)$ is not zero only when $\theta(s)$ reaches the value 0 or π, which implies a discontinuity of ψ and φ in $[\,0, 2\pi\,[$.

The value $\psi(0)$ is the precession angle of the Frenet frame at $s = 0$,

$$\psi(0) = \begin{cases} 0 & \text{if } \sin\theta(0) = 0 \\ \text{sign}\left(t_P - (a-u_3)\dfrac{\lambda}{2}\right)\dfrac{\pi}{2} & \text{otherwise} \end{cases}. \tag{2.44}$$

The value $\varphi(0) \in [\,0, 2\pi\,[$ is chosen arbitrarily: it is the reference for the angular position of the Darboux frame around $\boldsymbol{t} = \boldsymbol{d}_3$.

System (2.41) gives the orientation of sections parametrized by the three constants $\{\lambda, t_P, a\}$. Note that both the trajectory and the orientation of sections can also be conveniently expressed with five other parameters $\{z_1, z_2, z_3, sg_1, sg_2\}$[26] (see Appendix C).

2. Expression of angle $\zeta = (\widehat{\boldsymbol{n}, \boldsymbol{d}_1})$

Another way to define the orientation of sections is to express the angle $\zeta = (\widehat{\boldsymbol{n}, \boldsymbol{d}_1})$ that orientates the Darboux frame in the Frenet frame around the tangent $\boldsymbol{t} = \boldsymbol{d}_3$. This angle is such that[31,32]

$$\dot{\zeta}(s) = \Omega_t - t_G, \tag{2.45}$$

where t_G is the geometric torsion, defined as

$$t_G = -\dot{\boldsymbol{b}} \cdot \boldsymbol{n}. \tag{2.46}$$

With this sign convention, right-handed helices have a constant positive t_G. Using the equation of equilibrium (2.9b) to calculate $\dot{\boldsymbol{b}}$, it is possible to demonstrate that[16]

$$t_G(s) = \frac{1}{2}\left(t_P - \frac{2\lambda - (a + \lambda^2 - t_P^2)t_P}{\kappa^2(s)}\right), \tag{2.47}$$

where $\kappa^2(s)$ is given by the square of (2.22)

$$\kappa^2(s) = u(s) + \lambda^2 - t_P^2. \tag{2.48}$$

Integration of Eq. (2.45) gives

$$\zeta(s) = \zeta(0) + \left(\frac{K_0}{K_3} - \frac{1}{2}\right) t_P\, s + \frac{2\lambda - (a + \lambda^2 - t_P^2)t_P}{2c_\Psi \kappa^2(0)} \Pi(n_\zeta, \Psi(s), m) + \zeta_{cor}(s), \tag{2.49}$$

with

$$n_\zeta = (u_3 - u_2)/\kappa^2(0), \tag{2.50}$$

$$\zeta_{cor}(s) = \begin{cases} \left(\lfloor s/s_{per} - 1/2 \rfloor + 1\right)\pi & \text{if } \; t_G = u_2 = 0 \quad \text{and} \quad u_1 u_3 \neq 0 \\ 0 & \text{otherwise} \end{cases}. \tag{2.51}$$

The correction $\zeta_{cor}(s)$ takes care of the singularities of 2D trajectories at inflexion points. The value $\zeta(0) \in [\,0, 2\pi\,[$ is chosen arbitrarily: it is the reference for the angular position of the Darboux frame around $\boldsymbol{t} = \boldsymbol{d}_3$.

E. Symmetry of elastic rods

An important property of elastic rods is their symmetry through the transformation $\{\lambda, t_P, a\} \longrightarrow \{-\lambda, -t_P, a\}$. With definition (2.26) of $p_3(u)$, we observe that this transformation leaves $p_3(u)$ unchanged, and the roots $\{u_1, u_2, u_3\}$ are therefore unchanged. Considering the equations of trajectory (2.34)

$$\{\rho, \phi, z\} \longrightarrow \{\rho, -\phi, z\}, \tag{2.52}$$

thus we obtain the symmetric trajectory with respect to plane $\{O, \boldsymbol{e}_i, \boldsymbol{e}_k\}$. This symmetry also bears on the Darboux frame, as we see with Eq. (2.49) that

$$\zeta(s) - \zeta(0) \longrightarrow -(\zeta(s) - \zeta(0)). \tag{2.53}$$

III. DOMAIN OF DEFINITION

Differential Eq. (2.25) can be solved if and only if there exists an interval $D_u \subset \mathbb{R}^+$ such that

$$\forall\, u \in D_u, \quad p_3(u) \geq 0. \tag{3.1}$$

D_u can be reduced to a single real value. The polynomial $p_3(u)$ is expressed in (2.26), and its sign is readily obtained for large $|u|$: it is positive when $u \longrightarrow -\infty$ and negative when $u \longrightarrow +\infty$. To study more precisely the sign of $p_3(u)$, we discuss its discriminant Δ defined in (2.29).

If $\Delta < 0$ then $p_3(u)$ has only one simple real root, which is negative. This invalidates condition (3.1), excepted when the real root is null, which implies that $D_u = \{0\}$ can be chosen to obtain straight rods: the results exposed in Subsection IV A show that these trajectories are not pertinent because all straight rods are located in another region. As a consequence, Eq. (2.25) requires $\Delta \geq 0$. In this case, $p_3(u)$ has three real roots and with (2.28c) we note that u_1 is negative, and u_2 and u_3 are of the same sign (we show in the supplementary material that $u_3 = 0$ implies $u_2 = 0$). Thus, condition (3.1) is satisfied if and only if u_3 is positive, by taking $D_u = [u_2, u_3]$. As Δ and u_3 are functions of $\{\lambda, t_P, a\}$, this implies that $\{\lambda, t_P, a\}$ evolve within a domain of definition $\mathfrak{D} \subset \mathbb{R}^3$ defined by

$$(\lambda, t_P, a) \in \mathfrak{D} \Longleftrightarrow \begin{cases} \Delta(\lambda, t_P, a) \geq 0 \\ \text{and} \\ u_3(\lambda, t_P, a) \geq 0 \end{cases}. \tag{3.2}$$

As λ and t_P are related to the force and moment that are imposed to the rod, they vary in all $\mathbb{R}$. Thus, condition (3.2) only bears on a. With the same argument and considering the definition of a in (2.17), this parameter cannot be bounded by an upper value. However, the condition $||\boldsymbol{r}'(s)|| = 1$ readily leads to $a \geq -2$. As a consequence, the domain of definition $\mathfrak{D}$ is searched in the form

$$a \geq a_{Min}(\lambda, t_P) \geq -2, \tag{3.3}$$

where $a_{Min}(\lambda, t_P)$ is obtained by resolving system (3.2).

A. Positive discriminant Δ

Δ is a fourth-degree polynomial of a (see Appendix D). To solve $\Delta(\lambda, t_P, a) \geq 0$, we study its four roots $\{a_1, a_2, a_3, a_4\}$. These roots $a_k(\lambda, t_P)$ are expressed analytically in Appendix D. We choose to classify them as when the four are real, $a_1 \leq a_2 \leq a_3 \leq a_4$. Then when only two of them are real, they are named a_1 and a_4. This is done numerically.

In the case $t_P = -\lambda$, Δ has only one double real root

$$a_1(\lambda, -\lambda) = a_4(\lambda, -\lambda) = -2. \tag{3.4}$$

When $t_P = \lambda$, Δ has four real roots shown in Fig. 2. In the general case, when $t_P \neq \pm\lambda$, Δ possesses at least two real roots, and all its roots are plotted in Fig. 3. Note that the plots are symmetric with

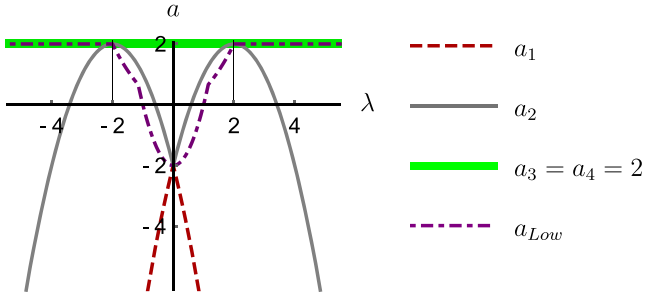

FIG. 2. Plot of the real roots $\{a_1, a_2, a_3, a_4\}$ of the discriminant Δ superposed to a plot of a_{Low}, as functions of λ in the case $t_P = \lambda$. When $\lambda \in]-\infty, -2[\cup]2, +\infty[$, the condition $a \geq a_{Low}$ implies that $a \in]-\infty, a_3 = a_4[$ is excluded, so that the domain of definition is $a \in [\, a_4, +\infty\,[$. When $\lambda \in [-2, 2]$, $a \in]-\infty, a_1]$ is not allowed by $a \geq a_{Low}$, and $a \in [\, a_1, a_2\,[$ is forbidden by $\Delta \geq 0$: in this case, the domain of definition is $a \in [\, a_2, +\infty\,[$.

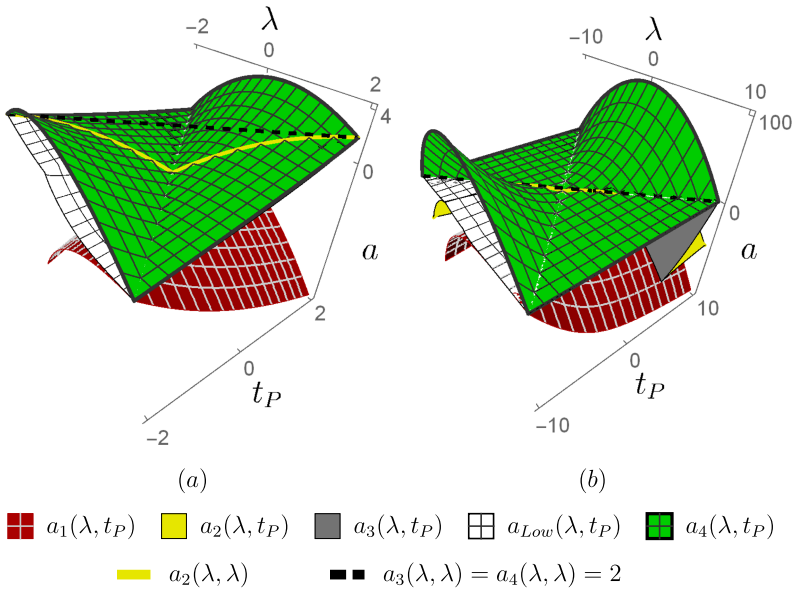

FIG. 3. Plots of the roots $\{a_1, a_2, a_3, a_4\}$ of the discriminant Δ superposed to a plot of the value a_{Low}, as functions of λ and t_P: $\lambda \in [-b, b]$, $t_P \in [-b, b]$, and $a \in [-2b^2, b^2]$ where $b = 2$ in plot (a) and $b = 10$ in plot (b). As implicitly shown in these plots, when $t_P \neq \pm\lambda$, the surface $a_{Low}(\lambda, t_P)$ is always located below $a_4(\lambda, t_P)$ and above $a_3(\lambda, t_P)$. As a result, the condition $a \geq a_{Low}$ forbids the interval $a \in]-\infty, a_3]$ and the domain of definition is $a \in [\, a_4, +\infty\,[$. See the supplementary material for interactive view.

respect to the axis $\lambda = t_P = 0$. This is due to the invariance of Δ with respect to the transformation $\{\lambda, t_P, a\} \longrightarrow \{-\lambda, -t_P, a\}$, visible in (2.29).

This knowledge of the roots of Δ lets us construct Table I representing the variations of the sign of $\Delta(\lambda, t_P, a)$. Seven cases are derived according to the number of real roots and their multiplicity. We see that in all cases, Δ is positive for $a \in\,]-\infty, a_1\,] \cup [\, a_4, +\infty\,[$. In some cases, $a \in [a_2, a_3]$ also implies that Δ is positive, but all other parts of $\mathbb{R}$ are forbidden.

B. Positive root u_3

To complete the resolution of system (3.2), it is necessary to solve $u_3 \geq 0$. Assume that $\Delta \geq 0$, then $\{u_1, u_2, u_3\}$ are real, u_1 is negative, and u_2 and u_3 are of the same sign. Thus, it suffices that one root is positive to ensure that u_3 is positive. Descartes's rule of signs guarantees that there are as many positive roots of $p_3(u)$ as there are changes of signs in the sequence $(\varepsilon_{3-k})_{k\in\{0,1,2,3\}}$ of the coefficients of $p_3(u)$ defined in (2.27) and ordered by decreasing subscript (ignoring null ε_k coefficients). As we only need to identify one positive root, applying Descartes's rule of signs leads directly to

$$\Delta(\lambda, t_P, a) \geq 0 \;\text{ and }\; u_3(\lambda, t_P, a) \geq 0 \iff \Delta(\lambda, t_P, a) \geq 0 \;\text{ and }\; a \geq a_{Low}(\lambda, t_P), \tag{3.5}$$

where

$$a_{Low}(\lambda, t_P) = \begin{cases} \lambda^2 - \sqrt{4 - 4\lambda t_P + \lambda^4} & \text{if } \lambda \neq 0 \text{ and } \left(t_P - 1/\lambda - 3/16\lambda^3\right)\lambda < 0 \\ \lambda^2/2 & \text{if } \lambda \neq 0 \text{ and } \left(t_P - 1/\lambda - 3/16\lambda^3\right)\lambda \geq 0 \\ -2 & \text{if } \lambda = 0 \end{cases}. \tag{3.6}$$

The solution to the whole system (3.2) stems from both requirements $\Delta \geq 0$ (Table I) and (3.5). When $t_P = -\lambda$, we note that $a_{Low} = a_1 = a_4 = -2$ and therefore that $a \in [\, a_4, +\infty\,[$ is the domain of definition. Figure 2 shows that in the case $t_P = \lambda$, for $\lambda^2 > 4$, condition $a \geq a_{Low}(\lambda, t_P)$ forbids a to be in $]-\infty, a_3\,[$ and condition $\Delta \geq 0$ (see Table I) requires $a \in [\, a_3 = a_4, +\infty\,[$; for $\lambda^2 \leq 4$, $a \in [\, a_2, a_3\,[$ also belongs to the domain of definition. Finally, Fig. 3 shows that a is restrained to $[\, a_4, +\infty\,[$ when $t_P \neq \pm\lambda$.

TABLE I. Variations of the sign of $\Delta(\lambda, t_P, a)$: "+" stands for $\Delta > 0$, "−" for $\Delta < 0$.

				$t_P = -\lambda$					
Case 1				$a_1 = a_4 = -2$					
$t_P = -\lambda \neq 0$	+			0					+
1 double root									
				$t_P = \lambda$					
Case 2			$a_1 = a_2 = -2$				$a_3 = a_4 = 2$		
$t_P = \lambda = 0$	+		0		+		0		+
2 double roots									
Case 3		a_1				$a_2 = a_3 = a_4 = 2$			
$t_P = \lambda = \pm 2$	+	0		−		0			+
1 simple and 1 triple roots									
Case 4		a_1		a_2			$a_3 = a_4 = 2$		
$0 \neq t_P = \lambda \neq \pm 2$	+	0	−	0	+		0		+
2 simple and 1 double roots									
				$t_P \neq \pm\lambda$					
Case 5		a_1		a_2		a_3		a_4	
4 simple roots	+	0	−	0	+	0	−	0	+
Case 6		a_1			$a_2 = a_3$			a_4	
2 simple and 1 double roots	+	0	−		0		−	0	+
Case 7		a_1						a_4	
2 simple roots	+	0			−			0	+

As a conclusion, the domain of definition $\mathfrak{D}$ is such that

$$(\lambda, t_P, a) \in \mathfrak{D} \iff \begin{cases} (\lambda, t_P) \in \mathbb{R}^2 \\ a \in [\ a_{Min}(\lambda, t_P), +\infty\ [\end{cases}, \tag{3.7}$$

where

$$a_{Min}(\lambda, t_P) = \begin{cases} a_2(\lambda, t_P) & \text{if } \ t_P = \lambda \in [-2, 2] \\ a_4(\lambda, t_P) & \text{otherwise} \end{cases}. \tag{3.8}$$

This important result is not unexpected as it generalizes the well-known domain of definition of the Euler elastica to the ideal 3D elastica.

IV. PARTICULAR TRAJECTORIES

With the formalism presented in Sec. II and the definition domain obtained in Sec. III, it is possible to position each particular geometry in the $\{\lambda, t_P, a\}$ space and to characterize them precisely. This is done by imposing geometric constraints on ideal elastic rods and by resolving the resulting equations as functions of parameters $\{\lambda, t_P, a\}$.

A. 1D-2D shapes, helices, homoclinics

Thus, straight rods are obtained for $\kappa = cst = 0$, circles for $z(s)$ constant, 2D elastica for $\phi(s)$ piecewise constant, helices for $m = 0$, and homoclinics for $m = 1$. In each case, equations of trajectory (2.34) are reduced and geometric characteristics are identified. Details are given in the supplementary material and lead to the classification presented in Table II.

One particularly remarkable result is that the lower bound of the definition domain, $a_{Min}(\lambda, t_P)$, is also the surface of all helices. In Fig. 4, the radius and pitch of these helices are plotted as functions of λ and t_P, where surface $a_{Min}(\lambda, t_P)$ is divided in four regions with alternate pitch signs. Another

TABLE II. Location and characterization of particular trajectories. The first two columns are equivalent and entail the last two columns. The reverse does not necessarily hold true.

Trajectories	Location	Roots of $p_3(u)$	Characteristics
Straight lines	$t_P = a\lambda/2$ $a = \pm 2$	$u_2\ u_3 = 0$	Torsion angle density $\Omega_t = (K_0/K_3)t_P$ Tension if $a = 2$, compression if $a = -2$
Circles	$\lambda = \pm 1/\sqrt{a}$ $t_P = 1/\lambda$ $a > 0$	$u_2 = u_3 = a$	Radius $\rho_0 = \sqrt{a}$ Torsion angle density $\Omega_t = (K_0/K_3)t_P$
Inflexional 2D elastica	$t_P = \lambda = 0$ $-2 \le a < 2$	$u_1 = a - 2$ $u_2 = 0$ $u_3 = a + 2$	$m = (2 + a)/4$ $m \in [0, 1]$
Non-inflexional 2D elastica	$t_P = \lambda = 0$ $a \ge 2$	$u_1 = 0$ $u_2 = a - 2$ $u_3 = a + 2$	$m = 4/(2 + a)$ $m \in [0, 1]$
Helices	$a = a_{Min}(\lambda, t_P)$	$u_2 = u_3$	Radius $\rho_0 = \sqrt{\frac{1}{3}\left(2a - \lambda^2 + \sqrt{-3p}\right)}$ Pitch $p_z = 2\pi \frac{(a - \rho_0^2)\rho_0^2}{\lambda\rho_0^2 + 2t_P - a\lambda}$ p defined in (2.30)
Homoclinics	$\lambda^2 < 4$ $t_P = \lambda$ $a = 2$	$u_1 = u_2 = 0$	Maximal radius $\rho_{max} = \sqrt{4 - \lambda^2}$

important result is that given the values of radius ρ_0 and pitch p_z, there are two helices distinguished by $sg = \pm 1$,

$$\lambda = \frac{\rho_0 p_z + sg\, 2\pi\, \kappa\, l_t}{2\pi\, \rho_0}, \quad t_P = \frac{p_z\, \kappa + sg\, 2\pi\, \rho_0\, l_t}{2\pi\, \rho_0}, \quad \kappa = cst = \frac{\rho_0}{\rho_0^2 + \left(\frac{p_z}{2\pi}\right)^2}. \tag{4.1}$$

In Fig. 5, the trajectories of Table II are shown in $\{\lambda, t_P, a\}$ space.

B. Closed shapes

Dichmann *et al.* proposed for the first time a complete bifurcation diagram for closed rods.[21] Here, we demonstrate that in the formalism of Landau, these particular shapes are embedded in a parametrized surface defined analytically.

1. Equations

Closed shapes are obtained when the trajectory $\boldsymbol{r}(s)$ and the Darboux frame are periodic and have the same period. Equations (2.34), (2.35), (2.49), and (2.51) and the properties of elliptic functions and elliptic integrals tell that for all $(s_0, q_z) \in \mathbb{R} \times \mathbb{Z}^*$,

$$\begin{cases} z(s_0 + q_z s_{per}) = z(s_0) + q_z\, z(s_{per}), & \text{(4.2a)} \\ \phi(s_0 + q_z s_{per}) = \phi(s_0) + q_z\, \phi(s_{per}), & \text{(4.2b)} \\ \zeta(s_0 + q_z s_{per}) = \zeta(s_0) + q_z\, \zeta(s_{per}) - q_z\, \zeta(0), & \text{(4.2c)} \end{cases}$$

where s_{per} is the period of $u = \rho^2$ defined in (2.36). From these equations,

$$z \text{ periodic} \iff z(s_{per}) = 0 \iff z \text{ periodic of period } s_{per}, \tag{4.3a}$$

$$\{x, y\} \text{ periodic of period } q_z s_{per} \iff \exists\, q_\phi \in \mathbb{Z}, \quad \phi(s_{per}) = 2\pi q_\phi / q_z, \tag{4.3b}$$

$$\{\boldsymbol{d}_\mu\} \text{ periodic of period } q_z s_{per} \iff \exists\, q_\zeta \in \mathbb{Z}, \quad \zeta(s_{per}) = \zeta(0) + 2\pi q_\zeta / q_z. \tag{4.3c}$$

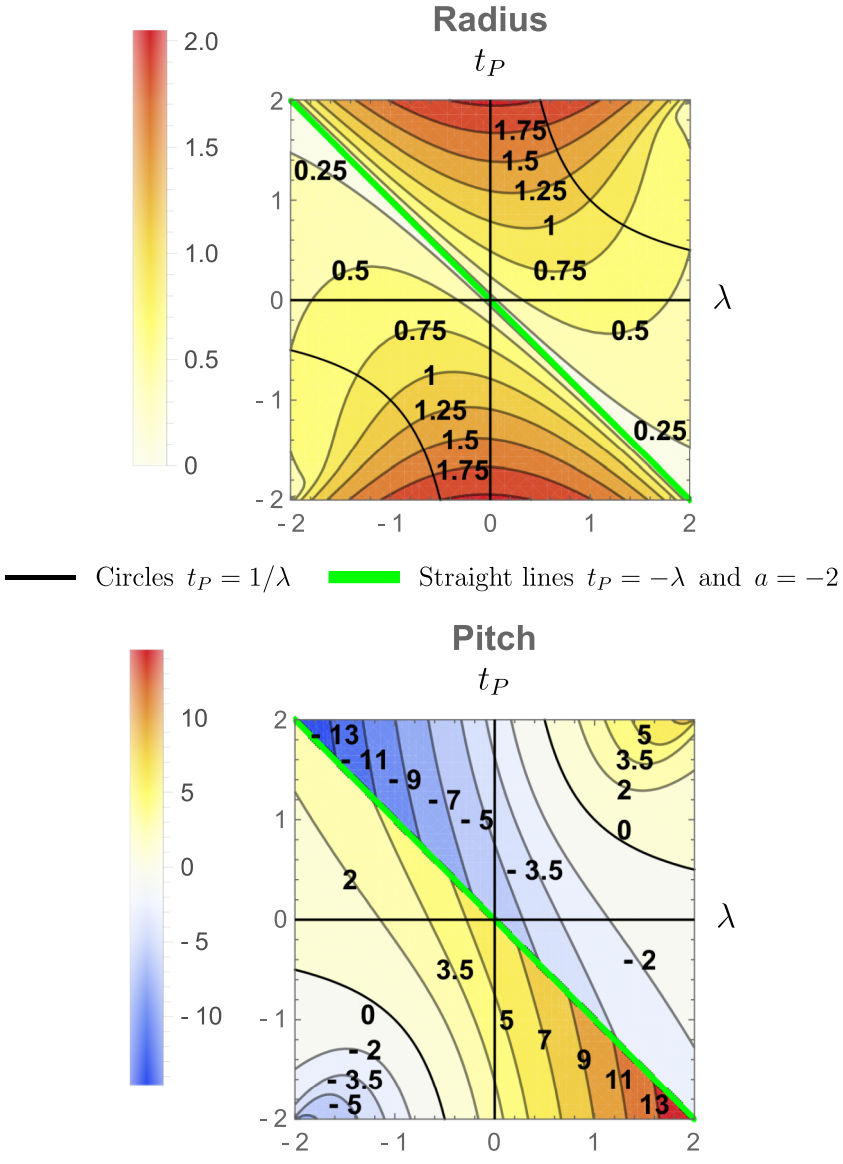

FIG. 4. Radius and pitch of helices as functions of λ (abscissa) and t_P (ordinate).

Using (2.34) and (2.49), we deduce that an ideal elastic rod is closed if and only if there exists three integers $\{q_z, q_\phi, q_\zeta\}$ such that

$$\begin{cases} c_\Psi z(s_{per}) = (a-u_1)K(m) - (u_3-u_1)E(m) = 0, & \text{(4.4a)} \\ \phi(s_{per}) = \dfrac{u_3\lambda K(m) + (2t_P - a\lambda)\Pi(n,m)}{u_3\, c_\Psi} + \phi_{cor}(s_{per}) = 2\pi\dfrac{q_\phi}{q_z}, & \text{(4.4b)} \\ \zeta(s_{per}) - \zeta(0) = \\ \qquad \left(\dfrac{K_0}{K_3} - \dfrac{1}{2}\right) t_P s_{per} + \dfrac{t_P - 2t_G(0)}{c_\Psi}\Pi(n_\zeta, m) + \zeta_{cor}(s_{per}) = 2\pi\dfrac{q_\zeta}{q_z}. & \text{(4.4c)} \end{cases}$$

Another set of equations can be obtained, involving Euler angles (ψ, θ, φ). Indeed, it has been demonstrated in Ref. 26 that during one period s_{per} of $z(s)$, the cylindrical coordinate ϕ and the Euler angle of precession ψ have congruent angular variations modulo 2π. The same result stands for ζ and φ. As a consequence, conditions $\phi(s_{per}) = 2\pi q_\phi/q_z$ and $\zeta(s_{per}) = \zeta(0) + 2\pi q_\zeta/q_z$ in, respectively, (4.4b)

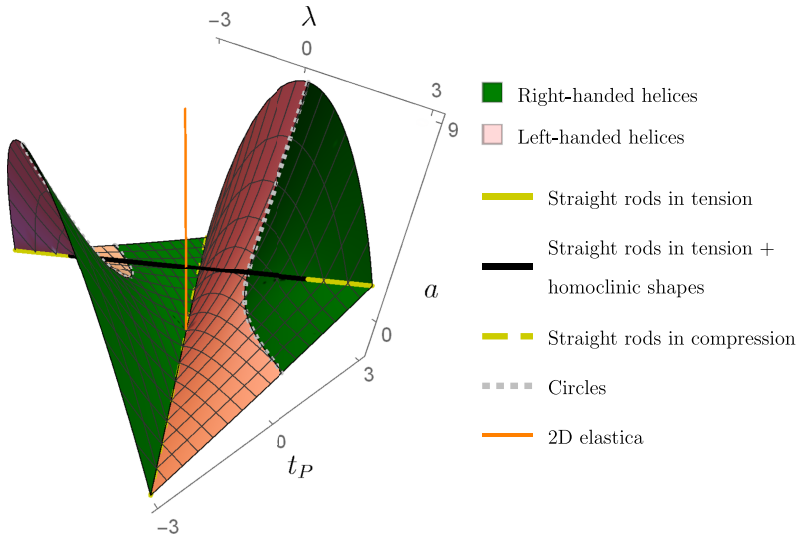

FIG. 5. Plot of the regions of $\{\lambda, t_P, a\}$ space corresponding to null discriminant ($\Delta = 0$) and to the specific case of 2D elastica ($\lambda = t_P = 0$). The region $\Delta = 0$ includes right- and left-handed helices ($a = a_{Min}(\lambda, t_P)$), straight rods ($a = \pm 2$ and $t_P = a\lambda/2$), circles ($a = a_{Min}(\lambda, t_P)$ and $t_P = 1/\lambda$), and homoclinic trajectories ($a = 2$ and $-2 < t_P = \lambda < 2$). See the supplementary material for interactive view.

and (4.4c) can be replaced equivalently by $\psi(s_{per}) = \psi(0) + 2\pi q_\psi/q_z$ and $\varphi(s_{per}) = \varphi(0) + 2\pi q_\varphi/q_z$, where q_ψ and q_φ are integers. With Eq. (2.41), this leads to

$$\begin{cases} c_\Psi z(s_{per}) = (a - u_1)K(m) - (u_3 - u_1)E(m) = 0, & \text{(4.5a)} \\ \psi(s_{per}) - \psi(0) = 2(\psi_P^+ + \psi_P^-) + \psi_{cor}(s_{per}) = 2\pi \dfrac{q_\psi}{q_z}, & \text{(4.5b)} \\ \varphi(s_{per}) - \varphi(0) = \left(\dfrac{K_0}{K_3} - 1\right) t_P\, s_{per} + 2(\psi_P^+ - \psi_P^-) + \psi_{cor}(s_{per}) = 2\pi \dfrac{q_\varphi}{q_z}, & \text{(4.5c)} \end{cases}$$

where

$$\psi_P^+ = \frac{\lambda + t_P}{(2 + a - u_3)c_\Psi}\Pi\left(n^+, m\right), \quad \psi_P^- = \frac{\lambda - t_P}{(2 - a + u_3)c_\Psi}\Pi\left(n^-, m\right). \tag{4.6}$$

n^+ and n^- are defined in (2.43).

2. Practical computation

We approximate the dense discrete set of closed shapes in the $\{\lambda, t_P, a\}$ space by the embedding surface generated by Eq. (4.5a). This is a good approximation because $\mathbb{Q}$ is dense in $\mathbb{R}$, hence there can always be found a rational q_ψ/q_z that solves Eq. (4.5b) with any desired precision. Furthermore, there is always one value of K_0/K_3 that solves Eq. (4.5c).

To solve Eq. (4.5a), it is useful to introduce the following variables:[26]

$$\begin{cases} z_1 = \dfrac{1}{2}(a - u_3), & \text{(4.7a)} \\ z_2 = \dfrac{1}{2}(a - u_2), & \text{(4.7b)} \\ z_3 = \dfrac{1}{2}(a - u_1). & \text{(4.7c)} \end{cases}$$

With these parameters, Eq. (4.5a) becomes

$$(z_3 - z_1)E(m) + z_3 K(m) = 0. \tag{4.8}$$

The modulus m of Eq. (2.32) can be equivalently expressed as

$$m = \frac{z_2 - z_1}{z_3 - z_1}. \tag{4.9}$$

Appendix C explains how to obtain the parameters $\{\lambda, t_P, a\}$ from $\{z_1, z_2, z_3\}$ and the signs sg_1 and sg_2 of $\lambda + t_P$ and $\lambda - t_P$, respectively. Thus, the approximate space of closed shapes can be parametrized by $\{m, z_3, sg_1, sg_2\}$. We obtain the red surface in Fig. 7. All exact closed shapes are embedded in this surface, which is a remarkably simple result compared to what was obtained, for instance, in Refs. 21 and 25. Note the symmetry with respect to axis $\lambda = t_P = 0$, explained by the invariance of Eq. (4.5a) with respect to the transformation $\{\lambda, t_P, a\} \longrightarrow \{-\lambda, -t_P, a\}$ (by the same arguments as in Sec. II E).

V. GENERAL CASE

To classify the shapes in the general case, we have identified geometric properties that characterize all elastic rods.

A. General geometric properties of elastic rods

1. The elastic rods wind around a core helix

First, we observe through Eqs. (4.2a), (4.2b), and (2.34) that $z(s)$ and $\phi(s)$ oscillate around linear functions. It is therefore possible to introduce a core helix around which the 3D elastic shapes are wound. We define this helix by its trajectory

$$\boldsymbol{r}_H(s_H) = x_H(s_H)\boldsymbol{e}_i + y_H(s_H)\boldsymbol{e}_j + z_H(s_H)\boldsymbol{e}_k, \tag{5.1}$$

as

$$\begin{cases} x_H(s_H) = \rho_H \cos(c_\phi s_H), & \text{(5.2a)} \\ y_H(s_H) = \rho_H \sin(c_\phi s_H), & \text{(5.2b)} \\ z_H(s_H) = c_z s_H, & \text{(5.2c)} \end{cases}$$

where

$$\rho_H = \frac{\sqrt{u_3} + \sqrt{u_2}}{2}, \quad c_\phi = \frac{\phi(s_{per})}{s_{per}} = \frac{\lambda}{2} + \frac{2t_P - \lambda a}{2u_3}\frac{\Pi(n,m)}{K(m)}, \tag{5.3}$$

$$c_z = \frac{z(s_{per})}{s_{per}} = \frac{1}{2}(a - u_1) - \frac{u_3 - u_1}{2}\frac{E(m)}{K(m)}. \tag{5.4}$$

Under this definition, $||\dot{\boldsymbol{r}}_H(s_H)|| = \sqrt{\rho_H^2 c_\phi^2 + c_z^2} \neq 1$, so that s_H is not the arc length.

In the case $m = 0$, the rod has a helical trajectory (given in the supplementary material) that corresponds also to the core helix. A singularity is obtained when $u_3 = 0$, where c_ϕ is not defined. As this corresponds to straight lines, we choose $c_\phi = 0$ in this case.

When $n = 1$, which is equivalent to $u_2 = 0$, c_ϕ is not defined. However, generating a Taylor series expansion of c_ϕ about $n = 1$ to zeroth order and using (2.28c), for $m \neq 1$ it follows that

$$c_\phi \underset{n=1}{\approx} \frac{\lambda}{2} + \text{sign}(2t_P - \lambda a)\frac{\pi}{4}\frac{\sqrt{-u_1}}{\sqrt{1-m}K(m)}. \tag{5.5}$$

With Eq. (2.28c), we see that the sign of $2t_P - \lambda a$ changes when $u_2 = 0$, implying a step change of c_ϕ. It is therefore possible to extend the definition of c_ϕ by choosing arbitrarily $\text{sign}(2t_P - \lambda a) = 1$ in Eq. (5.5).

When $n = 1$ and $m = 1$, Eq. (5.5) with $u_1 = (m-1)u_3/m$ gives

$$c_\phi \underset{m=1}{\underset{n=1}{\approx}} \frac{\lambda}{2}. \tag{5.6}$$

As there is no discontinuity in this case, Eq. (5.6) extends c_ϕ continuously.

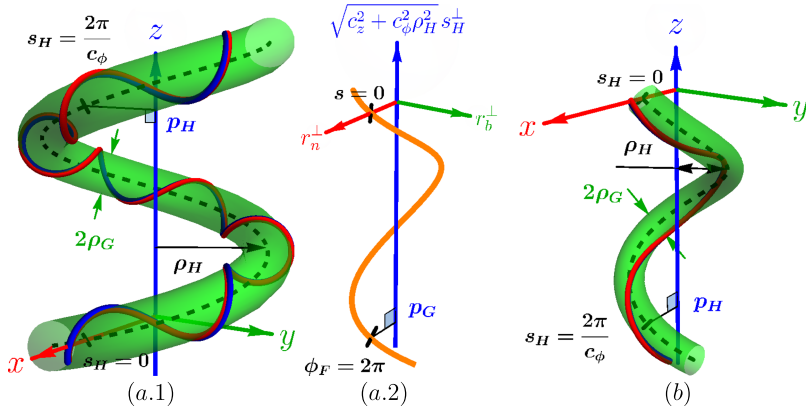

FIG. 6. Two examples showing the global structure of 3D elastic shapes. In example (a), the trajectory is plotted in the global reference frame $\{O, \boldsymbol{e}_i, \boldsymbol{e}_j, \boldsymbol{e}_k\}$ in (a.1) and in the Frenet frame $\{\boldsymbol{r}_H(s_H^\perp), -\boldsymbol{n}_H(s_H^\perp), -\boldsymbol{b}_H(s_H^\perp), \boldsymbol{t}_H(s_H^\perp)\}$ of the core helix in (a.2). In example (b), it is only plotted in the global reference frame. The thick dashed lines are the core helices about axis z, right-handed in (a) ($S_H = +1$) and left-handed in (b) ($S_H = -1$). The elastic rods wind around these helices with a negative sign in (a) ($S_G = -1$) and a positive sign in (b) ($S_G = +1$). As shown by the multicolored thin tubes, the rods are, respectively, negatively twisted in (a) ($S_P = -1$) and positively in (b) ($S_P = +1$). The elastic trajectories are contained in a tube-shaped envelope.

Hence we have exhibited the existence of a core helix for each elastic trajectory, with radius given by (5.3) and pitch p_H defined as

$$p_H = z_H\left(s_H = \frac{2\pi}{c_\phi}\right) = \frac{2\pi c_z}{c_\phi}. \tag{5.7}$$

The observation that elastic trajectories wind around a helix has been proposed previously, even in cases of non-ideal 3D rods.[26,27]

2. The elastic rods are contained in a tube-shaped envelope

Second, the choice we have made for ρ_H implies that elastic trajectories are always contained within a tube-shaped envelope whose centre line is the core helix. Examples are shown in Fig. 6. The radius ρ_G of this tube is

$$\rho_G = \frac{\sqrt{u_3} - \sqrt{u_2}}{2}. \tag{5.8}$$

Noting $\{\boldsymbol{n}_H, \boldsymbol{b}_H, \boldsymbol{t}_H\}$ the Frenet basis of the core helix, the tube-shaped envelope is defined by its surface $\boldsymbol{r}_{tube}(s_H, \alpha)$,

$$\boldsymbol{r}_{tube}(s_H, \alpha) = \boldsymbol{r}_H(s_H) + \rho_G \cos(\alpha)\boldsymbol{n}_H + \rho_G \sin(\alpha)\boldsymbol{b}_H\,,\ \alpha \in [0, 2\pi]. \tag{5.9}$$

3. The elastic rods have a second pitch p_G

Third, it is possible to plot the elastic trajectories in the Frenet frame of their core helix. Let $s_H^\perp(s)$ be the curvilinear abscissa of the orthogonal projection of the point $\boldsymbol{r}(s)$ on the core helix. The coordinates $(r_n^\perp, r_b^\perp, r_t^\perp)$ of the point $\boldsymbol{r}(s)$ in the Frenet frame $\{\boldsymbol{n}_H(s_H^\perp), \boldsymbol{b}_H(s_H^\perp), \boldsymbol{t}_H(s_H^\perp)\}$ are given by

$$\begin{cases} r_n^\perp(s) = \rho_H - \rho(s)\cos\left(\phi(s) - c_\phi s_H^\perp\right), & \text{(5.10a)} \\ r_b^\perp(s) = \dfrac{-c_z\,\rho(s)\sin\left(\phi(s) - c_\phi\, s_H^\perp\right) + \left(z(s) - c_z\, s_H^\perp\right) c_\phi \rho_H}{\sqrt{c_z^2 + c_\phi^2\,\rho_H^2}}, & \text{(5.10b)} \\ r_t^\perp(s) = c_\phi\,\rho_H \sin\left(\phi(s) - c_\phi\, s_H^\perp\right) + \left(z(s) - c_z s_H^\perp\right) c_z = 0. & \text{(5.10c)} \end{cases}$$

The abscissa $s_H^\perp(s)$ is obtained by resolving numerically Eq. (5.10c).

The curve

$$\boldsymbol{r}_F(s) = r_n^\perp(s)\,\boldsymbol{n}_H(0) + r_b^\perp(s)\,\boldsymbol{b}_H(0) + \sqrt{c_z^2 + c_\phi^2\rho_H^2}\,s_H^\perp \boldsymbol{t}_H(0) \tag{5.11}$$

gives the elastic trajectory in the Frenet frame of the core helix. The cylindrical coordinates (ρ_F, ϕ_F, z_F) are used to describe this curve, with $-r_n^\perp = \rho_F\cos(\phi_F)$ and $-r_b^\perp = \rho_F\sin(\phi_F)$. $\phi_F(s) \in \mathbb{R}$ is continuous for every trajectory that does not intersect the core helix, and it is such that $\phi_F(0) = 0$.

Equations (5.3), (5.4), and (5.10) imply that $s_H^\perp(s_{per}) = s_{per}$ and that $\phi_F(s)$ makes one turn during one period s_{per}. It is therefore possible to define a pitch p_G as

$$p_G = z_F\begin{pmatrix}\phi_F = 2\pi \\ s = \pm s_{per}\end{pmatrix} = \pm\sqrt{c_z^2 + c_\phi^2\rho_H^2}\,s_{per}. \tag{5.12}$$

The sign of p_G can be obtained by writing the condition for an elastic trajectory to intersect its core helix. With (5.10), this condition is

$$\exists\, s \in \mathbb{R},\ r_n^\perp(s) = r_b^\perp(s) = 0 \quad \Longleftrightarrow \quad c_z\,\phi(s_0) - c_\phi\,z(s_0) = 0, \tag{5.13}$$

with

$$s_0 = \frac{1}{c_\Psi}\mathrm{sn}^{-1}\left(\sqrt{\frac{u_3 - \rho_H^2}{u_3 - u_2}}, m\right).$$

Trajectories that hold (5.13) true never hold $\phi_F = 2\pi$ true for any abscissa s: they are transitional trajectories for which the sign of the pitch cannot be defined. Furthermore, it can be observed that

$$\mathrm{sign}\,(p_G) = \mathrm{sign}(c_z\,\phi(s_0) - c_\phi\,z(s_0)). \tag{5.14}$$

4. The elastic rods have three chirality components

Fourth, 3D elastic rods are chiral, which means that they cannot be superimposed onto their mirror image. We identify three chirality components for every elastic rod:

(i) The core helix has a chirality S_H, i.e., it can be right-handed ($S_H = +1$) or left-handed ($S_H = -1$). S_H is the sign of the pitch p_H;
(ii) Elastic rods wind around their core helix with a chirality S_G, i.e., their trajectory in the Frenet frame of their core helix can be right-handed ($S_G = +1$) or left-handed ($S_G = -1$). S_G is the sign of the pitch p_G;
(iii) Cross sections turn around $\boldsymbol{t}$ with a chirality S_P, i.e., they are subjected to a positive ($S_P = +1$) or negative ($S_P = -1$) torsional moment $\boldsymbol{M}(s)\cdot\boldsymbol{t}$. S_P is the sign of t_P.

B. Classification of elastic rods according to chirality

Bending or turning one way or the other is at the roots of bifurcation theory. Here, this defines 2^3 distinct chiral classes. To make the classification precise, we need to plot in the $\{\lambda, t_P, a\}$ space the surfaces that correspond to a change of chirality components. Trivially, the plane $t_P = 0$ is one of them, related to S_P.

1. Change of chirality component S_H

A change of chirality component S_H corresponds to a sign change of the pitch p_H. According to (5.7), such a modification can occur when c_z or c_ϕ changes sign. c_z changes sign when the pitch p_H is null and the core helix is a circle: this has already been treated with closed shapes through Eq. (4.5a) and leads to a surface shown in Fig. 7. c_ϕ may change sign continuously or through a step change. The continuous change occurs when $c_\phi = 0$, i.e., when the core helix is a straight line: the corresponding surface in the $\{\lambda, t_P, a\}$ space is generated numerically and plotted in Fig. 7. As seen in Subsubsection V A 1, the discontinuous change of sign of c_ϕ may occur when $u_2 = 0$. Solving equation $u_2 = 0$ is achieved with (2.28) and conditions $u_1 \le 0 \le u_2 \le u_3$ and $a \ge -2$,

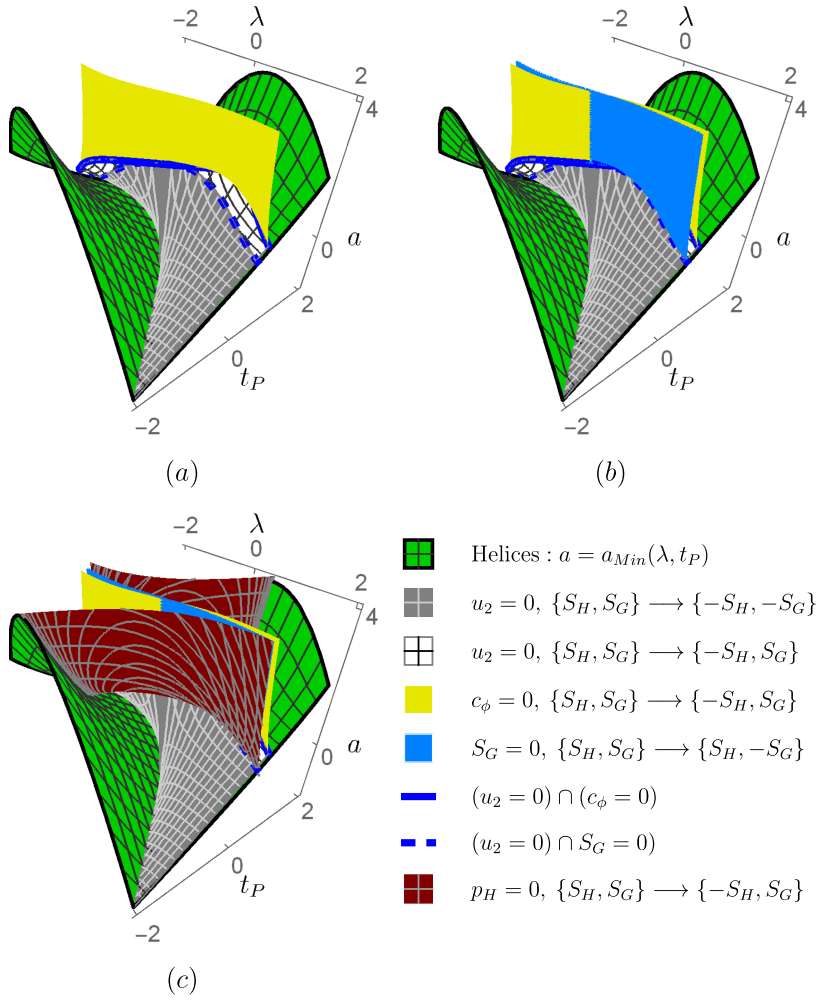

FIG. 7. Plots of the surfaces that delimit the bifurcation frontiers of chirality components $\{S_H, S_G\}$. The surface $a = a_{Min}(\lambda, t_P)$ of helices defines the lower bound of allowed $\{\lambda, t_P, a\}$ space. (a) The part of surface $u_2 = 0$ (discontinuous change of sign of c_ϕ) that corresponds to a change of chirality and the whole surface $c_\phi = 0$ (continuous change of sign of c_ϕ, where the core helix is a straight line). (b) With addition of the surface $S_G = 0$ of trajectories that intersect their core helix. (c) With addition of the surface $p_H = 0$ of approximate closed curves, for which the core helix is a circle. The transformations corresponding to these surfaces are given in the legend. See the supplementary material for interactive view.

$$(\lambda, t_P, a) \in \mathfrak{D} \quad \text{and} \quad u_2 = 0 \iff t_P = \frac{a\lambda}{2} \quad \text{and} \quad -2 \le a \le 2. \tag{5.15}$$

Then, we need to determine when $u_2 = 0$ implies a discontinuous change of sign of c_ϕ. This is done by computing the intersection between cases $u_2 = 0$ and $c_\phi = 0$, which with Eq. (5.5) yields the line

$$u_2 = 0 \quad \text{and} \quad \frac{\lambda}{2} = \pm\frac{\pi}{4}\frac{\sqrt{-u_1}}{\sqrt{1-m}K(m)}. \tag{5.16}$$

Note that equations $u_2 = 0$ and $c_\phi = 0$ are invariant with respect to the transformation $\{\lambda, t_P, a\} \longrightarrow \{-\lambda, -t_P, a\}$. Therefore, their intersection is symmetric with respect to axis $\lambda = t_P = 0$. In addition, we see in Fig. 7 that $c_\phi = 0$ occurs only when λ and t_P have the same sign. With Eq. (5.15) this also implies that $a \ge 0$. Considering these properties, we first compute the part $\{\lambda \ge 0, t_P \ge 0\}$ of the line (5.16) and obtain the part $\{\lambda \le 0, t_P \le 0\}$ by symmetry. Using (5.16) and (2.28), we arrive at the

following equations parametrized by $m \neq 1$,

$$\lambda = \frac{2\pi}{\left(\pi^4 + 8(2m-1)\pi^2 K(m)^2 + 16K(m)^4\right)^{1/4}}, \tag{5.17}$$

$$u_1 = -\frac{16(1-m)K(m)^2}{\left(\pi^4 + 8(2m-1)\pi^2 K(m)^2 + 16K(m)^4\right)^{1/2}}, \tag{5.18}$$

$$u_3 = \frac{m}{m-1}u_1\,,\ a = \sqrt{4+u_1 u_3}\,,\ t_P = \frac{a\lambda}{2}. \tag{5.19}$$

The case $m = 1$ adds only the point $\{\lambda = 0, t_P = 0, a = 2\}$ to the line defined by Eqs. (5.17)–(5.19). This line is the intersection between $c_\phi = 0$ and $u_2 = 0$, shown in Fig. 7. It is an important border, as only the part of the surface $u_2 = 0$ below this line (i.e., with lower values of a) corresponds to a change of chirality component S_H.

2. Change of chirality component S_G

Chirality component S_G is the sign of the pitch p_G, given in Eq. (5.14). As for chirality component S_H, a change of S_G can occur continuously or through the step change of c_ϕ induced by $u_2 = 0$. The surface corresponding to the continuous change is computed numerically and shown in Fig. 7. As no chirality S_G can be defined for the related trajectories, we impose $S_G = 0$ in this surface. To obtain the discontinuous change of S_G, the intersection between surfaces $S_G = 0$ and $u_2 = 0$ has to be plotted: it is a line computed numerically and shown in Fig. 7. The part of the surface $u_2 = 0$ below this line (i.e., with lower values of a) corresponds to a change of chirality component S_G.

3. Classification

As a result, the $\{\lambda, t_P, a\}$ space is subdivided into ten regions of constant chirality components $\{S_H, S_G, S_P\}$. Figure 8 is a sectional drawing for $t_P \leq -\lambda$. Because the representation of the delimiting surfaces is complex, the plane $t_P = 0$ for S_P is not displayed. The symmetry with respect to axis $\lambda = t_P = 0$ is used to deduce the part $t_P \geq -\lambda$ from the transformation $\{\lambda, t_P, a\} \longrightarrow \{-\lambda, -t_P, a\}$ that gives $\{S_H, S_G\} \longrightarrow \{-S_H, -S_G\}$.

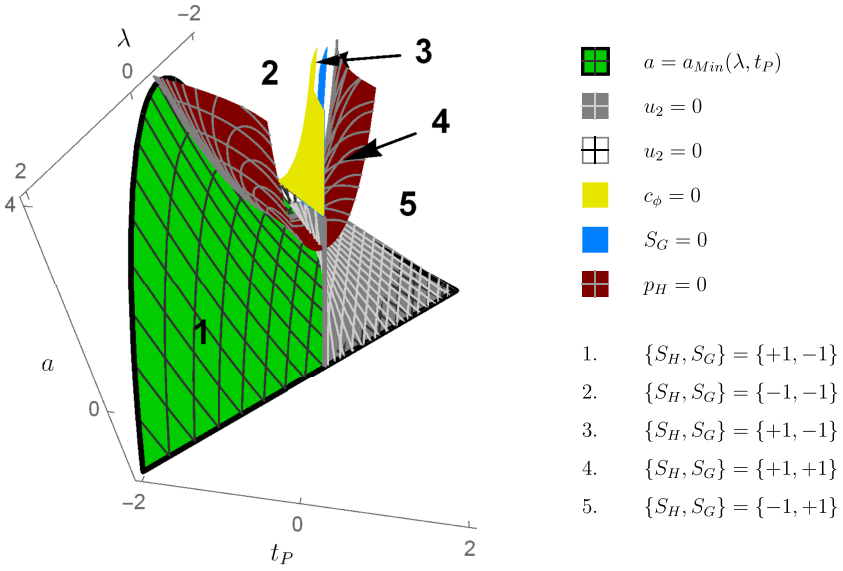

FIG. 8. Sectional plot of chiral classes $\{S_H, S_G\}$ in the $\{\lambda, t_P, a\}$ space, for $t_P \leq -\lambda$. The transformation $\{\lambda, t_P, a\} \longrightarrow \{-\lambda, -t_P, a\}$ gives the region $t_P \geq -\lambda$ through $\{S_H, S_G\} \longrightarrow \{-S_H, -S_G\}$. Superposing the plane $t_P = 0$ leads to the whole bifurcation diagram $\{S_H, S_G, S_P\}$.

C. Classification of elastic rods according to tube-shaped envelope

For a more precise classification, we decompose ideal elastic rods in classes with an identical tube-shaped envelope. The geometry of such an envelope is fully characterized by $\{\rho_H, \rho_G, p_H\}$, respectively, the radius of the core helix, the radius of the tube, and the pitch of the core helix. It is possible to find all elastic rods that correspond to a set of these parameters. This is done by obtaining analytically the parameters $\{\lambda, t_P, a\}$ as functions of $\{\rho_H, \rho_G, a\}$ and plotting the relation between a and p_H for constant $\{\rho_H, \rho_G\}$.

To obtain $\{\lambda, t_P, a\}$ as functions of $\{\rho_H, \rho_G, a\}$, we first express u_2 and u_3 as

$$u_2 = (\rho_H - \rho_G)^2\,,\ u_3 = (\rho_H + \rho_G)^2. \tag{5.20}$$

Then we use Eq. (2.28) and obtain four remarkably simple expressions of λ,

$$\lambda_{k\in\{1,2\}} = (-1)^{k+1}\frac{\sqrt{(4-(a-u_2)^2)u_2} - \sqrt{(4-(a-u_3)^2)u_3}}{u_3 - u_2}, \tag{5.21}$$

$$\lambda_{k\in\{3,4\}} = (-1)^{k+1}\frac{\sqrt{(4-(a-u_2)^2)u_2} + \sqrt{(4-(a-u_3)^2)u_3}}{u_3 - u_2}. \tag{5.22}$$

Therefore there exists four elastic rods (possibly identical) related to one set of $\{\rho_H, \rho_t, a\}$. They are not defined when $u_2 = u_3$, but this case corresponds to simple helices and has been fully treated in Subsection IV A and the supplementary material.

With Eq. (2.28a), the expressions of u_1 can be obtained as ($k \in \{1, 2, 3, 4\}$),

$$u_{1k} = 2a - u_2 - u_3 - \lambda_k^2. \tag{5.23}$$

When $\lambda_k \neq 0$ with $k \in \{1, 2, 3, 4\}$, Eq. (2.28b) gives

$$t_{Pk} = \frac{4 - a^2 + u_{1k}u_2 + u_{1k}u_3 + u_2u_3 + 2a\lambda_k^2}{4\lambda_k}. \tag{5.24}$$

When $\lambda_k = \lambda_{k+1} = 0$ with $k \in \{1, 3\}$, we use Eq. (2.28c) and arrive at

$$t_{Pk} = \frac{1}{2}\sqrt{-u_{1k}u_2u_3}\,,\quad t_{Pk+1} = -\frac{1}{2}\sqrt{-u_{1k}u_2u_3}. \tag{5.25}$$

Equations (5.21)–(5.25) give the four elastic rods related to $\{\rho_H, \rho_G, a\}$. Yet, not all values of $\{\rho_H, \rho_G, a\}$ are allowed. With Eqs. (2.25a) and (5.20) and the condition $||\dot{\boldsymbol{r}}(s)|| = 1$, we find two equivalent systems (the first for $\{u_2, u_3, a\}$, the second for $\{\rho_H, \rho_G, a\}$),

$$\begin{cases} \max(0, u_3 - 4) \le u_2 \le u_3 \\ \text{and} \\ -2 \le u_3 - 2 \le a \le u_2 + 2 \end{cases} \iff \begin{cases} 0 \le \rho_H\rho_G \le 1 \\ \text{and} \\ (\rho_H + \rho_G)^2 - 2 \le a \le (\rho_H - \rho_G)^2 + 2 \end{cases}. \tag{5.26}$$

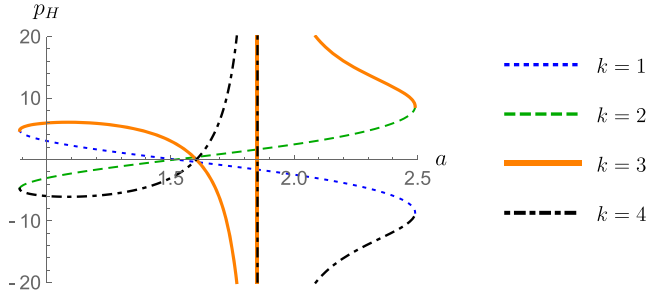

FIG. 9. Plot of the pitch p_H of the core helix as a function of a, for $\rho_H = 1.2$ and $\rho_G = 0.5$. For a given value of a, there exists four solutions $\{\lambda_k, t_{Pk}, a\}$ (possibly identical) expressed in Eqs. (5.21)–(5.25). For a given value of p_H, there are at most four corresponding elastic rods, for which the value of a can be obtained numerically. The vertical lines $a \simeq 1.86$ are the asymptotes of the curves $k = 3$ and $k = 4$. See the supplementary material for interactive view.

We thus have parametrized the geometries of elastic rods by $\{\rho_H, \rho_G, a\}$. For constant $\{\rho_H, \rho_G\}$, a only modifies the pitch p_H and the function $p_H(a)$ can be easily plotted: a typical example is shown in Fig. 9. Finally, all rods corresponding to one class $\{\rho_H, \rho_G, p_H\}$ are obtained by intersecting the plots $p_H(a)$ with the value of p_H. This leads to a maximum of four elastic rods corresponding to a tube-shaped envelope. Then these rods can be discriminated by criterions like chirality components $\{S_H, S_G, S_P\}$ or m-modulus.

VI. CONCLUSIONS

The formalism introduced by Landau *et al.*,[28] developed by Tobias *et al.*[16] and that we have extended here gives the analytical expressions of infinite solution trajectories as functions of only three parameters $\{\lambda, t_P, a\}$. Furthermore, the orientation of sections and the mechanical loading are well described analytically with these parameters. We have shown how $\{\lambda, t_P, a\}$ are related to physical quantities. In particular, a represents the sum of the contribution of traction/compression and of the component of the moment orthogonal to the force.

The domain of definition $\mathfrak{D} \subset \mathbb{R}^3$ of the parameters $\{\lambda, t_P, a\}$ where the trajectories are defined is simply $a \geq a_{Min}(\lambda, t_P)$, $(\lambda, t_P) \in \mathbb{R}^2$. All particular geometries have been completely characterized and located in this domain, as shown in one single figure: straight lines, circles, 2D elastica, helices, and homoclinic trajectories.

As the global reference frame has been chosen so that all solutions are conveniently written in a cylindrical coordinate system with axis z, we have identified a general geometric structure for all elastic rods. All trajectories wind around a core helix and are contained in a tube-shaped envelope that we have both described analytically. This structure possesses three chirality properties that subdivide the $\{\lambda, t_P, a\}$ space in ten regions of constant chiralities $\{S_H, S_G, S_P\}$. As chirality properties have a dramatic incidence on the geometry, this space reduction should be useful to initiate numerical methods without divergences to solve trajectories of elastic rods.

Finally, the geometries of all elastic rods are expressed analytically in terms of three other parameters $\{\rho_H, \rho_G, a\}$ that provide a good geometric control of infinite trajectories through their envelope. With this, elastic rods are characterized by the parameters $\{\rho_H, \rho_G, p_z\}$ that define the geometry of the tube-shaped envelope. A diagram can always be generated analytically to describe precisely the relation between a and p_z for any given $\{\rho_H, \rho_G\}$.

All these results provide a more complete view of ideal 3D elastica. They give detailed expressions and tools to resolve the equilibrium of elastic rods in applied research. They open different perspectives to address important topics such as stability and structural stability.

SUPPLEMENTARY MATERIAL

See Supplementary material for two files. The first file contains the derivations of the results summarized in Table II and other developments: force-less configurations and relations between trajectories and Darboux reference frames. The second file provides interactive views of Figs. 3, 5, 7, and 9, as well as a general interactive explorer of trajectories. The latter requires Wolfram CDF Player, freely downloadable at http://www.wolfram.com/cdf-player/.

ACKNOWLEDGMENTS

The authors acknowledge support from the program "Convergence UPMC" and the Ph.D. program "Interface Pour le Vivant UPMC." They especially thank S. Neukirch and J.-M. Maillard for helpful discussions, as well as the referee for helpful recommendations.

APPENDIX A: ELLIPTIC FUNCTIONS

Here we give the expressions used for elliptic functions, with the modulus $m \in [0, 1]$ and the characteristic $n \in \mathbb{R}$.

1. Incomplete elliptic integrals

The incomplete elliptic integrals, respectively, of the first, second, and third kind are defined as

$$F(\Psi, m) = \int_0^{\Psi} \frac{d\overline{\Psi}}{\sqrt{1 - m\sin^2(\overline{\Psi})}}, \tag{A1}$$

$$E(\Psi, m) = \int_0^{\Psi} \sqrt{1 - m\sin^2(\overline{\Psi})}\, d\overline{\Psi}, \tag{A2}$$

$$\Pi(n, \Psi, m) = \int_0^{\Psi} \frac{d\overline{\Psi}}{\left(1 - n\sin^2(\overline{\Psi})\right)\sqrt{1 - m\sin^2(\overline{\Psi})}}. \tag{A3}$$

2. Complete elliptic integrals

The complete elliptic integrals, respectively, of the first, second, and third kind are defined as

$$K(m) = F\left(\frac{\pi}{2}, m\right), \quad E(m) = E\left(\frac{\pi}{2}, m\right), \quad \Pi(n, m) = \Pi\left(n, \frac{\pi}{2}, m\right). \tag{A4}$$

3. Jacobi's elliptic functions

The amplitude function of Jacobi is given by

$$\mathrm{am}(s, m) = (F^{-1})(s, m), \tag{A5}$$

and serves to define the functions sn, cn, and dn by

$$\mathrm{sn}(s, m) = \sin\left(\mathrm{am}(s, k)\right), \tag{A6}$$

$$\mathrm{cn}(s, m) = \cos\left(\mathrm{am}(s, k)\right), \tag{A7}$$

$$\mathrm{dn}(s, m) = \sqrt{1 - m\,\mathrm{sn}^2(s, k)}. \tag{A8}$$

APPENDIX B: RESOLUTION OF SYSTEM (2.40)

System (2.40) can be written as

$$\begin{cases} \dot{\psi}(s) = \dfrac{1}{2}\dfrac{\lambda + t_P}{1 + z_\theta} + \dfrac{1}{2}\dfrac{\lambda - t_P}{1 - z_\theta}, & \text{(B1a)} \\ \dot{\varphi}(s) = \left(\dfrac{K_0}{K_3} - 1\right) t_P + \dfrac{1}{2}\dfrac{\lambda + t_P}{1 + z_\theta} - \dfrac{1}{2}\dfrac{\lambda - t_P}{1 - z_\theta}, & \text{(B1b)} \\ z_\theta(s) = \dot{z}(s) = \dfrac{1}{2}(a - u) = \dfrac{a - u_3}{2} + \dfrac{u_3 - u_2}{2}\mathrm{sn}^2\left(c_\Psi s, m\right). & \text{(B1c)} \end{cases}$$

To solve this system, let us define

$$n^+ = -\frac{u_3 - u_2}{2 + a - u_3} \quad , \quad n^- = \frac{u_3 - u_2}{2 - a + u_3}. \tag{B2}$$

We arrive at

$$\begin{cases} \dot{\psi}(s) = \dfrac{\lambda + t_P}{2 + a - u_3}\dfrac{1}{1 - n^+\mathrm{sn}^2\left(c_\Psi s, m\right)} + \dfrac{\lambda - t_P}{2 - a + u_3}\dfrac{1}{1 - n^-\mathrm{sn}^2\left(c_\Psi s, m\right)} \\ \dot{\varphi}(s) = \left(\dfrac{K_0}{K_3} - 1\right) t_P + \dfrac{\lambda + t_P}{2 + a - u_3}\dfrac{1}{1 - n^+\mathrm{sn}^2\left(c_\Psi s, m\right)} - \dfrac{\lambda - t_P}{2 - a + u_3}\dfrac{1}{1 - n^-\mathrm{sn}^2\left(c_\Psi s, m\right)} \\ z_\theta(s) = \dfrac{a - u_3}{2} + \dfrac{u_3 - u_2}{2}\mathrm{sn}^2\left(c_\Psi s, m\right) \end{cases}. \tag{B3}$$

Integrating this system leads to the final expressions

$$\begin{cases} \psi(s) \equiv \psi(0) + \psi^+(s) + \psi^-(s) + \psi_{cor}(s) \quad [2\pi], & \text{(B4a)} \\ \theta(s) = \arccos\left(\dfrac{a-u_3}{2} + \dfrac{u_3-u_2}{2}\mathrm{sn}^2\left(c_\Psi s, m\right)\right), & \text{(B4b)} \\ \varphi(s) \equiv \varphi(0) + (K_0/K_3 - 1)\, t_P\, s + \psi^+(s) - \psi^-(s) + \psi_{cor}(s) \quad [2\pi], & \text{(B4c)} \end{cases}$$

with

$$\psi^+(s) = \frac{\lambda + t_P}{2 + a - u_3}\frac{1}{c_\Psi}\Pi\left(n^+, \Psi(s), m\right), \quad \psi^-(s) = \frac{\lambda - t_P}{2 - a + u_3}\frac{1}{c_\Psi}\Pi\left(n^-, \Psi(s), m\right), \tag{B5a}$$

$$\psi_{cor}(s) = \begin{cases} 0 & \text{if} \quad s = 0 \\ (1 + \mathrm{sign}(s))\,\pi/2 & \text{if} \quad m = 1 \text{ and } t_P = 0 \\ 0 & \text{if} \quad m = 1 \text{ and } t_P \neq 0 \\ \left(\lfloor s/s_{per} \rfloor + \lfloor s/s_{per} - 1/2 \rfloor + 2\right)\pi & \text{if} \quad u_2 = a-2 \text{ and } u_3 = a+2 \\ \left(\lfloor s/s_{per} \rfloor + 1\right)\pi & \text{if} \quad u_2 \neq a-2 \text{ and } u_3 = a+2 \\ \left(\lfloor s/s_{per} - 1/2 \rfloor + 1\right)\pi & \text{if} \quad u_2 = a-2 \text{ and } u_3 \neq a+2 \\ 0 & \text{otherwise} \end{cases}, \tag{B5b}$$

where $\lfloor \cdot \rfloor$ is the floor function. In Eq. (B5b), the conditions must be considered successively from the top to the bottom, and the first that holds true gives the value of $\psi_{cor}(s)$. This corrective term is used to take into account the discontinuity of ψ and φ when $\theta(s)$ reaches the value 0 or π.

APPENDIX C: PARAMETRIZATION WITH $\{z_1, z_2, z_3\}$

Following the work of Nizette and Goriely in Ref. 26, it can be useful to parametrize the solutions (2.34) and (2.41) by three quantities $\{z_1, z_2, z_3\}$. They are related to our set of variables by the following definitions

$$z_1 = \frac{1}{2}(a - u_3), \quad z_2 = \frac{1}{2}(a - u_2), \quad z_3 = \frac{1}{2}(a - u_1). \tag{C1}$$

As u_1, u_2, and u_3 are ordered when real, these definitions ensure that $z_1 \leq z_2 \leq z_3$. Giving these three parameters plus the sign sg_1 of $\lambda + t_P$ and the sign sg_2 of $\lambda - t_P$, we can deduce $\{\lambda, t_P, a\}$.

To do this, it is useful to introduce the following positive variables M_+ and M_-:

$$M_+ = sg_1\frac{\lambda + t_P}{2}, \quad M_- = sg_2\frac{\lambda - t_P}{2}. \tag{C2}$$

Equation (C2) can be written equivalently as

$$\lambda = sg_1 M_+ + sg_2 M_- \quad , \quad t_P = sg_1 M_+ - sg_2 M_-. \tag{C3}$$

Then, evaluating Eq. (2.26) with $u = a - 2$ and $u = a + 2$, we obtain

$$4(\lambda - t_P)^2 = (a - 2 - u_1)(a - 2 - u_2)(a - 2 - u_3), \tag{C4}$$

$$4(\lambda + t_P)^2 = (a + 2 - u_1)(a + 2 - u_2)(a + 2 - u_3). \tag{C5}$$

This leads to

$$(\lambda - t_P)^2 = 2(z_1 - 1)(z_2 - 1)(z_3 - 1), \tag{C6}$$

$$(\lambda + t_P)^2 = 2(z_1 + 1)(z_2 + 1)(z_3 + 1). \tag{C7}$$

Therefore, M_+ and M_- are

$$M_+ = \sqrt{\frac{(z_1 + 1)(z_2 + 1)(z_3 + 1)}{2}} \quad , \quad M_- = \sqrt{\frac{(z_1 - 1)(z_2 - 1)(z_3 - 1)}{2}}. \tag{C8}$$

Equations (C3) and (C8) lead to the expressions of λ and t_P as functions of $\{z_1, z_2, z_3\}$ and $\{sg_1, sg_2\}$. Finally, with Eq. (2.28a) we obtain a,

$$a = 2(z_1 + z_2 + z_3) - \lambda^2. \tag{C9}$$

APPENDIX D: ROOTS OF Δ

Using Eqs. (2.27)–(2.30), the discriminant Δ of the polynomial $p_3(u)$ is a fourth-degree polynomial of a,

$$\Delta(\lambda, t_P, a) = 16\left(a^4 + \mu_3 a^3 + \mu_2 a^2 + \mu_1 a + \mu_0\right), \tag{D1}$$

with

$$\begin{cases} \mu_3 = -t_P^2 + 3\lambda^2 \\ \mu_2 = -8 - 20\lambda t_P - 2\lambda^2 t_P^2 + 3\lambda^4 \\ \mu_1 = 36 t_P^2 + 18\lambda t_P^3 + 20\lambda^2 - 22\lambda^3 t_P - \lambda^4 t_P^2 + \lambda^6 \\ \mu_0 = 16 - 27 t_P^4 - 48\lambda t_P + 30\lambda^2 t_P^2 + 2\lambda^3 t_P^3 + \lambda^4 - 2\lambda^5 t_P \end{cases}. \tag{D2}$$

Here, we express its four roots $\{a_1, a_2, a_3, a_4\}$ through a method proposed by Lagrange. This method is particularly convenient to plot the solutions in the $\{\lambda, t_P, a\}$ space, as there are no singularities in the expressions. We finish by presenting the ordering of these roots, which is achieved numerically and is also important to obtain pertinent graphs.

1. Intermediate equation

The first step to obtain Lagrange's expressions is to solve the following cubic equation:

$$y^3 + 2p_1 y^2 + (p_1^2 - 4r_1)y - q_1^2 = 0, \tag{D3}$$

where

$$p_1 = -\frac{3}{8}\mu_3^2 + \mu_2 \quad , \quad q_1 = \left(\frac{\mu_3}{2}\right)^3 - \frac{\mu_2\mu_3}{2} + \mu_1, \tag{D4}$$

$$r_1 = -3\left(\frac{\mu_3}{4}\right)^4 + \frac{\mu_2\mu_3^2}{16} - \frac{\mu_1\mu_3}{4} + \mu_0. \tag{D5}$$

This is done by defining the discriminant Δ_{int} as

$$\Delta_{int} = -(4p_2^3 + 27q_2^2) \tag{D6}$$

where

$$p_2 = -\frac{1}{3}p_1^2 - 4r_1 \quad , \quad q_2 = -\frac{2}{27}p_1^3 + \frac{8}{3}p_1 r_1 - q_1^2. \tag{D7}$$

Then, Cardano's formula is used to express the solutions y_k ($k \in \{1, 2, 3\}$),

$$y_k = -\frac{2}{3}p_1 + j^k y_{01} + j^{-k} y_{02} \tag{D8}$$

with

$$j = \exp\left(i\frac{2\pi}{3}\right), \; y_{01} = \sqrt[3]{\frac{1}{2}\left(-q_2 + \sqrt{-\frac{\Delta_{int}}{27}}\right)}, \; y_{02} = \sqrt[3]{\frac{1}{2}\left(-q_2 - \sqrt{-\frac{\Delta_{int}}{27}}\right)}. \tag{D9}$$

Note that in these expressions, the cubic root of any number x_0 is defined as follows:

- The unique solution to $x^3 = x_0$ when $x_0 \in \mathbb{R}$;
- The number $\exp\left(\frac{1}{3}\mathrm{Ln}\, x_0\right)$ when $x_0 \in \mathbb{C} \setminus \mathbb{R}$.

2. Lagrange's expressions of the roots

Once given the intermediate solutions $\{y_1, y_2, y_3\}$, Lagrange's method leads to the following expressions $\{\overline{a}_1, \overline{a}_2, \overline{a}_3, \overline{a}_4\}$ of the roots of Δ:

$$\begin{cases} \overline{a}_1 = -\dfrac{\mu_3}{4} + \dfrac{1}{2}\left(-\sqrt{y_1} - \sqrt{y_2} + r\,(y_3)\right) \\ \overline{a}_2 = -\dfrac{\mu_3}{4} + \dfrac{1}{2}\left(-\sqrt{y_1} + \sqrt{y_2} - r\,(y_3)\right) \\ \overline{a}_3 = -\dfrac{\mu_3}{4} + \dfrac{1}{2}\left(\sqrt{y_1} - \sqrt{y_2} - r\,(y_3)\right) \\ \overline{a}_4 = -\dfrac{\mu_3}{4} + \dfrac{1}{2}\left(\sqrt{y_1} + \sqrt{y_2} + r\,(y_3)\right) \end{cases}, \tag{D10}$$

where

$$r\,(y_3) = \begin{cases} \sqrt{y_3} & \text{if} \quad q_1\sqrt{y_1}\sqrt{y_2}\sqrt{y_3} \le 0 \\ -\sqrt{y_3} & \text{if} \quad q_1\sqrt{y_1}\sqrt{y_2}\sqrt{y_3} > 0 \end{cases}. \tag{D11}$$

These expressions are functions of λ and t_P defined in $\mathbb{R}^2$ without any singularity; hence they can be easily plotted.

3. Ordering of the roots

Finally, we choose numerically the values $\{a_1, a_2, a_3, a_4\}$ among the solutions $\{\overline{a}_1, \overline{a}_2, \overline{a}_3, \overline{a}_4\}$ such that when the four roots are real, $a_1 \le a_2 \le a_3 \le a_4$. Then when only two roots are real, we impose that they are a_1 and a_4. This ordering leads to the most pertinent plot, as we demonstrate in Sec. III that elastic rods are most often defined for $a \ge a_4$.

[1] W. Tang, P. Lagadec, D. Gould, T. R. Wan, J. Zhai, and T. How, "A realistic elastic rod model for real-time simulation of minimally invasive vascular interventions," Visual Comput. **26**, 1157–1165 (2010).
[2] T. McMillen and P. Holmes, "An elastic rod model for anguilliform swimming," J. Math. Biol. **53**, 843–886 (2006).
[3] B. Qian, T. R. Powers, and K. S. Breuer, "Shape transition and propulsive force of an elastic rod rotating in a viscous fluid," Phys. Rev. Lett. **100**, 078101 (2008).
[4] M. Aydogdu, "Axial vibration of the nanorods with the nonlocal continuum rod model," Phys. E **41**, 861–864 (2009).
[5] S. Neukirch, B. Roman, B. de Gaudemaris, and J. Bico, "Piercing a liquid surface with an elastic rod: Buckling under capillary forces," J. Mech. Phys. Solids **55**, 1212–1235 (2007).
[6] A. Balaeff, L. Mahadevan, and K. Schulten, "Elastic rod model of a DNA loop in the *Lac* operon," Phys. Rev. Lett. **83**, 4900–4903 (1999).
[7] C. Bouchiat and M. Mézard, "Elastic rod model of a supercoiled DNA molecule," Eur. Phys. J. E **2**, 377–402 (2000).
[8] D. Swigon, B. D. Coleman, and I. Tobias, "The elastic rod model for DNA and its application to the tertiary structure of DNA minicircles in mononucleosomes," Biophys. J. **74**, 2515–2530 (1998).
[9] M. Baouendi, J. A. H. Cognet, C. S. Ferreira, S. Missailidis, J. Coutant, M. Piotto, E. Hantz, C. Hervédu Penhoat, "Solution structure of a truncated anti-MUC1 DNA aptamer determined by mesoscale modeling and NMR," FEBS J. **279**, 479–490 (2012).
[10] G. P. Santini, J. A. H. Cognet, D. Xu, K. K. Singarapu, and C. Herve du Penhoat, "Nucleic acid folding determined by mesoscale modeling and NMR spectroscopy: Solution structure of d(GC GAAA GC)," J. Phys. Chem. B **113**, 6881–6893 (2009).
[11] A. Goriely and M. Tabor, "Nonlinear dynamics of filaments I. Dynamical instabilities," Phys. D **105**, 20–44 (1997).
[12] G. Guhados, W. Wan, and J. L. Hutter, "Measurement of the elastic modulus of single bacterial cellulose fibers using atomic force microscopy," Langmuir **21**, 6642–6646 (2005).
[13] C. Storm, J. J. Pastore, F. C. MacKintosh, T. C. Lubensky, and P. A. Janmey, "Nonlinear elasticity in biological gels," Nature **435**, 191–194 (2005).
[14] E. L. Starostin, "Three-dimensional shapes of looped DNA," Meccanica **31**, 235–271 (1996).
[15] Y. Shi and J. E. Hearst, "The Kirchhoff elastic rod, the nonlinear Schrödinger equation, and DNA supercoiling," J. Chem. Phys. **101**, 5186–5200 (1994).
[16] I. Tobias, B. D. Coleman, and W. K. Olson, "The dependence of DNA tertiary structure on end conditions: Theory and implications for topological transitions," J. Chem. Phys. **101**, 10990–10996 (1994).
[17] S. S. Antman, *Nonlinear Problems of Elasticity*, Applied Mathematical Sciences, 2nd ed. (Springer, New York, 2005).
[18] G. Domokos and P. Holmes, "Euler's problem, Euler's method, and the standard map; or, the discrete charm of buckling," J. Nonlinear Sci. **3**, 109–151 (1993).
[19] G. van der Heijden and J. Thompson, "Helical and localised buckling in twisted rods: A unified analysis of the symmetric case," Nonlinear Dyn. **21**, 71–99 (2000).
[20] G. Domokos, "A group-theoretic approach to the geometry of elastic rings," J. Nonlinear Sci. **5**, 453–478 (1995).
[21] D. J. Dichmann, Y. Li, and J. H. Maddocks, "Hamiltonian formulations and symmetries in rod mechanics," in *Mathematical Approaches to Biomolecular Structure and Dynamics* (Springer Verlag, 1996), pp. 71–113.
[22] E. Starostin, "Symmetric equilibria of a thin elastic rod with self-contacts," Philos. Trans. R. Soc., A **362**, 1317–1334 (2004).
[23] N. Chouaieb, A. Goriely, and J. H. Maddocks, "Helices," Proc. Natl. Acad. Sci. U. S. A. **103**, 9398–9403 (2006).
[24] S. Neukirch and M. E. Henderson, "Classification of the spatial equilibria of the clamped elastica: Symmetries and zoology of solutions," J. Elasticity **68**, 95–121 (2002).

[25] M. E. Henderson and S. Neukirch, "Classification of the spatial equilibria of the clamped elastica: Numerical continuation of the solution set," Int. J. Bifurcation Chaos **14**, 1223–1239 (2004).
[26] M. Nizette and A. Goriely, "Towards a classification of Euler–Kirchhoff filaments," J. Math. Phys. **40**, 2830–2866 (1999).
[27] S. Kehrbaum and J. Maddocks, "Elastic rods, rigid bodies, quaternions and the last quadrature," Philos. Trans. R. Soc., A **355**, 2117–2136 (1997).
[28] L. D. Landau, E. M. Lifshitz, A. M. Kosevich, and L. P. Pitaevskiĭ, *Theory of Elasticity*, Course of Theoretical Physics, 3rd ed. (Pergamon Press, 1986), Vol. 7.
[29] Wolfram Research, Inc., Mathematica 10.0, Wolfram Research, Inc., 2014.
[30] D. Cox, *Galois Theory, Pure and Applied Mathematics: A Wiley Series of Texts, Monographs and Tracts* (Wiley, 2012).
[31] B. D. Coleman, E. H. Dill, M. Lembo, Z. Lu, and I. Tobias, "On the dynamics of rods in the theory of Kirchhoff and Clebsch," Arch. Ration. Mech. Anal. **121**, 339–359 (1993).
[32] A. E. H. Love, *A Treatise on the Mathematical Theory of Elasticity* (Cambridge University Press, 1893), Vol. 2.